Thesis for the Master's degree in chemistry

Farinaz Kahnamouei

Effects of Temperature and Salt Addition on the Self-assembling Behavior of a Charged Hydrophobically End-capped Amphiphilic Triblock Copolymer

60 study points

DEPARTMENT OF CHEMISTRY
Faculty of mathematics and natural sciences
UNIVERSITY OF OSLO 05/2014

Thesis for the Master's Degree in Chemistry

Effects of Temperature and Salt Addition on the Self-assembling Behavior of a Hydrophobically End-capped Charged Amphiphilic Triblock Copolymer

By: Farinaz Kahnamouei

Supervisors: Prof. Bo Nyström and Dr. Reidar Lund

DEPARTMENT OF CHEMISTRY
Faculty of Mathematics and Natural Sciences
UNIVERSITY OF OSLO
05/2014

"The important thing in science is not so much to obtain new facts as to discover new ways of thinking about them"

Sir William Bragg

Contents

List of Figures

List of Tables

List of symbols and acronyms

Symbols

$^1\mathrm{HNMR}$ Hydrogen-1 nuclear magnetic resonance spectroscopy

A_f Amplitude for fast relaxation time

A_s Amplitude for slow relaxation time

b Block

B Empirical factor

β Stretching exponent of fast mode in Kohlrausch-Williams-Watts (KWW) stretched exponential

b_c Bound coherent scattering length

C_{18} Octadecyl

χ Flory-Huggins parameter

c_{solute} Weight fraction of the solute

d Density

ε Dielectric constant

η_0 Viscosity of the solvent

η Viscosity of the solution

$f(Ka)$ Henry's function

f Weight fraction

G Gibbs free energy

$g^1(q,t)$ First-order electric field autocorrelation function

$g^2(q,t)$ Homodyne intensity autocorrelation function

γ Stretching exponent of slow mode in Kohlrausch-Williams-Watts (KWW) stretched exponential

Γ Gamma function

k_B Boltzmann constant

λ Wavelength of scattering light in a vacuum

M Molar concentration

$\mathrm{M_n}$ Number average molecular weight

$\mathrm{M_w}$ Weight average molecular weight

n Refractive index

q Wave vector

ρ Scattering length density

R_h Hydrodynamic radius

R_{hs} Hydrodynamic radius of the slow mode

R_{hf} Hydrodynamic radius of the fast mode

S Scattered intensity signal

T Temperature

τ Turbidity

τ_{fe} Fast relaxation time

τ_{se} Slow relaxation time

θ Scattering angle

U_E Electrophoretic mobility

V Apparent partial specific volume

ζ Zeta potential

Acronyms

AFFFF Asymmetric flow field-flow fractionation

CMC Critical micelle concentration

CMT Critical micelle temperature

DDS Drug delivery systems

DLS Dynamic light scattering

LCST Lower critical solution temperature

MALS Multi angle light scattering

mPEG Methoxypoly(ethylene glycol)

ODA Octadecylacrylate

PA Polyamide

PAA Poly(acrylic acid)

PAMPS Poly(2-acrylamido-2-methyl-1-propanesulfonic acid)

PDEAM Poly(*N*,*N*-diethylacrylamide)

PDI Polydispersity index

PEG Poly(ethylene glycol)

PEO Poly(ethylene oxide)

PMAA Poly(methacrylic acid)

PNIPAAm Poly(*N*-isopropylacrylamide)

PS Polystyrene

SANS Small-angle neutron scattering

SAXS Small-angle X-ray scattering

SLD Scattering length density

SLS Static light scattering

UCST Upper critical solution temperature

USANS Ultra-small angle neutron scattering

Acknowledgments

First and foremost, I would like to express my sincere gratitude to my adviser, Bo Nyström. Bo's incredible knowledge and expertise has always been a significant breakthrough at different stages of this project and in variety of scientific challenges I encountered. His supports, however, were not limited to the scientific domains. Since my early days of joining to the department, it was Bo who kindly and patiently assisted me with adaptation to the new working environment, culture and language. It was a great pleasure working with you Bo, Thank You.

I would like to gratefully thank my co-adviser, Dr. Reidar Lund. Reidar's remarkable contributions have been indispensable to the success and materialization of this project.

Furthermore, I sincerely appreciate the constructive and supportive role of the Polymer Research Group at University of Oslo in substantiating this thesis. In particular, I would like to thank Dr. Kaizheng Zhu, who synthesized the studied polymer in this dissertation and Dr. Shahla Bagherifam who was in my advisory committee during the first semester of my studies at the department.

Moreover, special thanks go to Dr. Kenneth Knudsen at IFE, Kjeller who provided me with access to SANS instrument.

Besides, I would like to thank my dear friends and colleagues at UIO, without them my journey in Norway could have never been more fun. Thank you Leva, Sara, Golnaz, Elahe, Neda I hope our friendship lasts forever. When it comes to my friends outside UIO, I shall gratefully thank Mohammad, Sajad, Safa, Saghi, Mehrad who supported me out and beyond distances that have kept us apart.

The last but not the least, I should express my deepest gratitude to those outside academic environments, my family. Though distant from me, their continuous supports and love have always been radiating positive energy in my life.

Abstract

Effects of Temperature and Salt Addition on the Self-assembling Behavior of a Hydrophobically End-capped Charged Amphiphilic Triblock Copolymer

by

Farinaz Kahnamouei

Master of Science in Polymer chemistry

University of Oslo, May 2014

Advisers: Prof. Bo Nyström and Dr. Reidar Lund

In this study, association properties of aqueous solutions of anionic thermo-responsive hydrophobically end-capped amphiphilic triblock terpolymer n-octadecyl-poly(ethylene glycol)-poly(*N*-isopropyl acrylamide)-*block*-poly(2-acrylamido- 2-methyl-1-propanesulfonic sodium), abbreviated as C_{18}-PEG_{10}-*b*-$PNIPAAm_{54}$-*b*-$PAMPS_{10}$, have been studied by means of zeta potential measurements, turbidimetry, dynamic light scattering (DLS), densitometry and small angle light scattering (SANS) at various temperatures, polymer concentrations, and salinities. This polymer exhibits lower critical solution temperature (LCST) owing to its PNIPAAm block. Increasing the ionic strength of the aqueous solutions leads to a decrease in the cloud point (CP) of the solutions which is an indication of enhanced aggregation due to the screening of Coulomb repulsions. The dynamic light scattering (DLS) data gives a detailed information about the interactions between intra-chain and inter-chain associations. The zeta-potential is augmented through temperatures due to increase in charge density. The effect of ionic strength induced by adding different amounts of NaCl on solutions of the applied triblock terpolymer has been examined by means of turbidimetry, dynamic light scattering , densitometry and small angle neutron scattering (SANS). By increasing the amount of added salt, the electrostatic interactions are screened out and increasing the temperature promotes the formation of large aggregates. It has been demonstrated by turbidimetry experiments that CP is depressed when the ionic strength is increased. The results from DLS and SANS also confirm that higher salt concentration result in the formation of large aggregates at elevated temperatures.

Chapter 1

Introduction

In this chapter, the aim is to highlight theoretical backgrounds and some recent results that involve polymeric systems which have helped us to elucidate our complicated system introduced in this study.

In the past few decades, there has been considerable interest in synthesis and characterization of amphiphilic block copolymers. The amphiphilic (amphi: of both kinds; philic: having an affinity for) nature of a block copolymer is defined in presence of a solvent selective for a certain block. Amphiphilic block copolymers have the ability to self-assemble into well-defined nano-structures in aqueous solutions [1–5].

Amphiphilic block copolymers may contain a block or blocks that are able to undergo structural changes resulting into the production of new smart materials in response to external stimuli [6]. In pursuit of this, materials which respond to different types of stimuli like temperature [7], ionic strength [8], pH [9,10] and more have been synthesized and are the subject of many studies. Among all, the most studied stimuli is temperature. When heated above a critical transition temperature, a lot of polymers exhibit lower critical solution temperature, LCST (see 1.3.2), or upper critical solution temperature, UCST behavior promoting reversible aggregation or dissolution, respectively. Great enthusiasm towards thermo-responsive polymers has been shown over decades and an incredible amount of work has been carried out to develop temperature sensitive polymers [11–15].

Poly(*N*-isopropylacrylamide), PNIPAAm, is probably the most studied temperature-responsive polymer. To date, many research groups have managed to synthesize and characterize [16, 17] various thermo-responsive amphiphilic copolymers containing PNIPAAm, which give LCST behavior to the polymeric solutions [18–22] and gels [23, 24]. In biomedical sciences, their ability to encapsulate hydrophobic drugs, has been attracting significant attention in drug delivery systems (DDS) [25,26]

as well as their industrial applications [27].
In the following, we will shed light on theoretical aspects of this work together with a bibliographic overview of thermo-responsive and charged amphiphilic block copolymers and their behavior in aqueous solutions.

1.1 Polymers, copolymers and their architecture

Polymers are chain-like molecules of the same repeating units named monomers [28,29]. Monomers are connected to each other via a strong covalent bond [29]. Polymeric chains can have various architectures. Figure 1.1 illustrates three architectures: a linear chain (a), a branched chain (b), and a cross-linked polymer (c) [28].

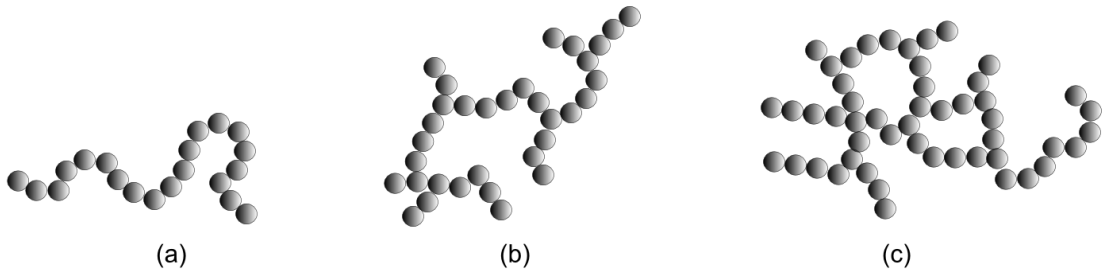

Figure 1.1: Polymer chain architecture: a linear chain (a), a branched chain (b), and a crosslinked polymer (c).

When synthesizing polymers, two or more different kinds of monomers could be employed and **copolymers** are formed. They possibly will be arranged randomly, or can form blocks and grafting branches; They are identified as random-, block-, and graft-copolymers respectively (Figure 1.2) [1, 29].

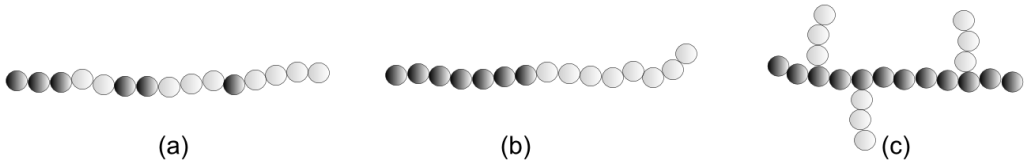

Figure 1.2: Different architectures of copolymers: a random copolymer (a), a block copolymer (b), and a graft copolymer (c).

Here, the focus is directed towards the block copolymers.

1.2 Amphiphilic block copolymers and self-assembly

Block copolymers in their selective solvents (a thermodynamical good solvent for one block and a precipitant for the other) form micelles or aggregates as a result of the association of insoluble blocks. In other words, as the insoluble segments accumulate, they create dense micellar cores which are then bounded by hydrophilic corona (soluble segments) followed by the micro-phase separation [2, 5, 30–33]. Due to the fact that the blocks are covalently linked together, the micro-phase separation is spatially limited which leads to the formation of self-assembled structures [5].

The micellar structures are formed above the critical micelle concentration (CMC), or above the critical micelle temperature (CMT) [34]. The amphiphilic block copolymers could naturally aggregate into a variety of nano-structures that are typically of spherical, cylindrical, or vesicular micelles. Figure 1.3 illustrates a diblock copolymer and some of its possible micellar structures in an aqueous solution [31, 35].

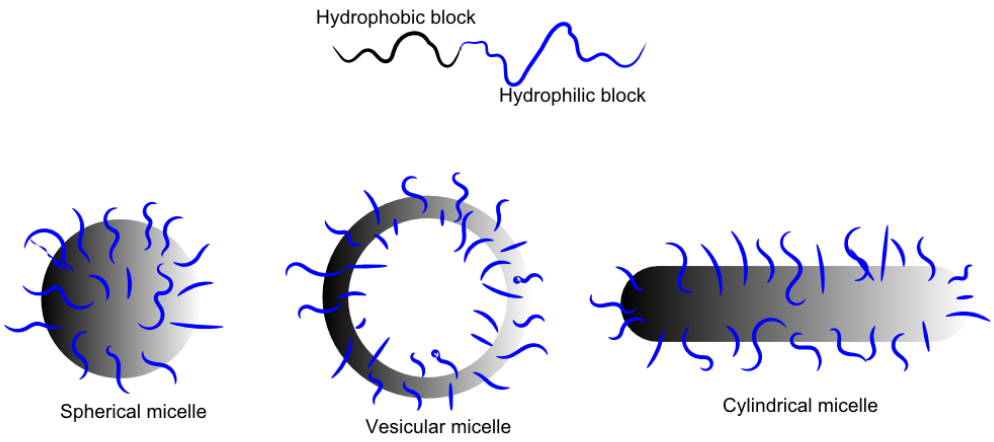

Figure 1.3: A diblock copolymer and its spherical, vesicular, and cylindrical micelles in aqueous medium

In amphiphilic diblock copolymers, aggregates are mostly spherical with core-shell structures named ”star” micelles, with the corona block being longer than the core. The aggregates are called ”crew cut” when the soluble block is much shorter (Figure 1.4) [8, 36]. In general, self-assembly into well-defined spherical core-shell micelle aggregates in aqueous solution is a characteristic that makes the amphiphilic block copolymers attractive to study [5].

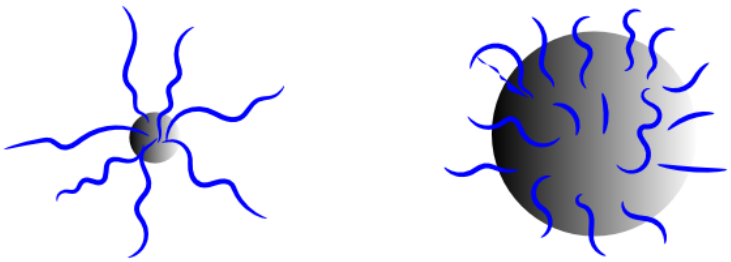

Figure 1.4: Starlike (left) and crew-cut (right) block copolymer micelles.

Yu et al [36] introduced preparation and observation of several morphologies of PS-*b*-PEO (polystyrene-*b*-polyethylene oxide) and PS-*b*-PAA (polystyrene-*b*-poly(acrylic acid)) crew-cut aggregates in dilute solutions. They were unique in their structures and hydrophilic surfaces, and some of them like porous spheres and interconnected rods have the potential to be used in drug delivery systems.

Graaf et al [37] have experimentally proved that the triblock copolymers with two hydrophobic blocks and a hydrophilic block in the middle self-assemble into flower-like micelles (Figure 1.5), i.e. the hydrophilic block is in a looped conformation. Flower-like micelles have lower CMC and higher kinetical stability in comparison with star-like micelles which makes them a better choice for drug delivery purposes. In a theoretical view, if the entropic penalty of the looping of the hydrophilic block is lower than the free energy decrease of micellization, the existence of the flower-like micelles is totally possible [38].

There are some factors that influence the final assembly structure, such as compatibilities between the two blocks described as the Flory-Huggins parameter (χ), rigidity of the blocks, and the volume fraction of each block in a certain polymer [3]. The physics behind the block copolymer phase behavior involves a competition between interfacial tension and the entropic penalty for stretching of polymeric coils in order to uniformly fill up the space. The balance determines the equilibrium size of the microdomains and dictates the geometry of the structure [39].

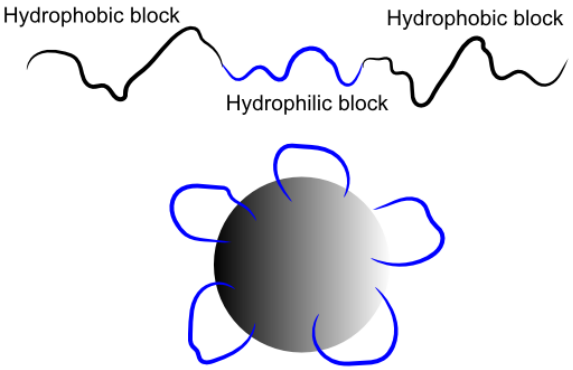

Figure 1.5: Flower like micelle

Since amphiphilicity is the chemical basis of self-assembly, and taken that the amphiphilicity of building blocks can be tuned, the process of self-assembly can be controlled to some extent. By tuning the amphiphilicity of building blocks, including small surfactants and amphiphilic copolymers, self-assembly and disassembly, can be controlled [3, 40]. A large number of amphiphilic block copolymer micelles has been made from AB diblock copolymers. Nevertheless, amphiphilic ABC triblock copolymers are of great interest due to the huge number of distinctive morphologies that have been found and studied so far in the bulk. Additionally, introducing the third block brings some intriguing new functionalities [3, 5].

Applications

Hydrophobically modified water-soluble block copolymers are composed of both water-soluble and water-insoluble segments (low degrees of hydrophobic groups). As a result of this amphiphilic characteristic of the polymers, they may act as effective rheology modifiers, and can therefore be utilized in several industrial applications where controlling the rheology of the solution is required, such as in, paints, foods, pharmaceuticals, enhanced oil recovery, etc. The dynamo of association process is the interaction among hydrophobic segments which reduces their exposure to water [1, 41].

Apart from all those applications, the constant progress of new drug delivery systems is driven by the necessity to maximize therapeutic activity while minimizing undesirable side effects. Drug delivery vehicles formed by self-assembly of amphiphilic block copolymers in aqueous solutions

have received extensive attention during the past decades for several reasons. First of all, hydrophobic drugs could be encapsulated in the core of the micelles. Besides, the hydrophilic blocks, mostly composed of poly(ethylene oxide) (PEO), are capable of establishing hydrogen bonds with the aqueous media and structuring a firm shell around the micellar core [2, 11, 42].
The polymer used for this study is a charged triblock copolymer with lower critical solution temperature (LCST) characteristics which is the main focus of the next parts.

1.3 Stimuli responsive amphiphilic block copolymers

Polymers that undergo rather large and sudden physical or chemical changes in response to minor variations in their environmental conditions are referred to as stimuli responsive polymers. They recognize the induced signal, and according to its magnitude alter the chain's conformation in response to the signal. Stimuli can be physical or chemical [12, 32, 43]. Ionic strength variation, chemical agent addition and pH changes are classified as chemical stimuli. These stimuli will alter the interactions between polymer chains and also between polymer chains and the solvent. Temperature changes, electric or magnetic field variations and mechanical stress are considered as physical stimuli. Physical stimuli change the molecular interactions at critical onset points [2, 43]. Some polymeric systems can be triggered by more than one kind of stimulus [2, 43]. poly(*N*-isopropylacrylamide) (PNIPAAm), poly(*N*,*N*-diethylacrylamide) (PDEAM), poly(acrylic acid) (PAA), poly(methacrylic acid) (PMAA) are some of the most known stimuli responsive polymers [13].

1.3.1 Ionic strength-responsive (ion-responsive) amphiphilic block copolymers

This class of polymers manifest unusual behavior as a result of the attractive Coulombic interactions between oppositely charged segments. By changing the ionic strength, polymer solubility and the size of the polymeric chains are exposed to change. [2, 5]. Kjøniksen et al [44] have studied the effect of ionic strength on the association behavior of a series of charged thermo-sensitive methoxypoly(ethylene glycol)-*block*-poly(*N*-isopropylacrylamide)-*block*-poly(4-styrenesulfonic acid sodium) triblock copolymers (MPEG_{45}-*b*-$\mathrm{PNIPAAm}_{\mathrm{n}}$-*b*-$\mathrm{P(SSS)}_{22}$) with different lengths of the PNIPAAm block in aqueous solutions. They have claimed that in the presence of low amount of salt, screening of the electrostatic interactions is dominant, however, as the ionic strength is increased (level of NaCl addition), the salt may increase the strength of the hydrophobic

interactions. In the Hofmeister series Cl^- ions are classified as kosmotropes (structure makers) and they can augment the hydrophobicity of the solute and this may result into salting-out effect of the polymer followed by macroscopic phase separation.

Block copolymers containing both polyelectrolyte and hydrophobic blocks (or hydrophobically end-capped polyelectrolytes) could be seen as ionic polymeric surfactants. The adsorption of hydrophobic blocks on a solid substrate along with their attachment to water-air and water-oil interfaces offers ascent to mono-layers or polyelectrolyte brushes shaped by water-soluble blocks. Such structures have been widely studied [8].

The hydrophobically modified polyelectrolytes can form micelle-like association aggregates of distinctive morphologies. The self assembly of charged block copolymers in the solution at concentrations above the CMC leads to the formation of aggregates with a dense hydrophobic core of insoluble blocks and an extended charged corona, which guarantees solvency of micelles in water. These aggregates are called "polyelectrolyte micelles" (Figure 1.6). Hinging on the geometry, the coronae of such micelles could be imagined as bended polyelectrolyte brushes or systematically branch (star or comb-like) polyelectrolytes [8].

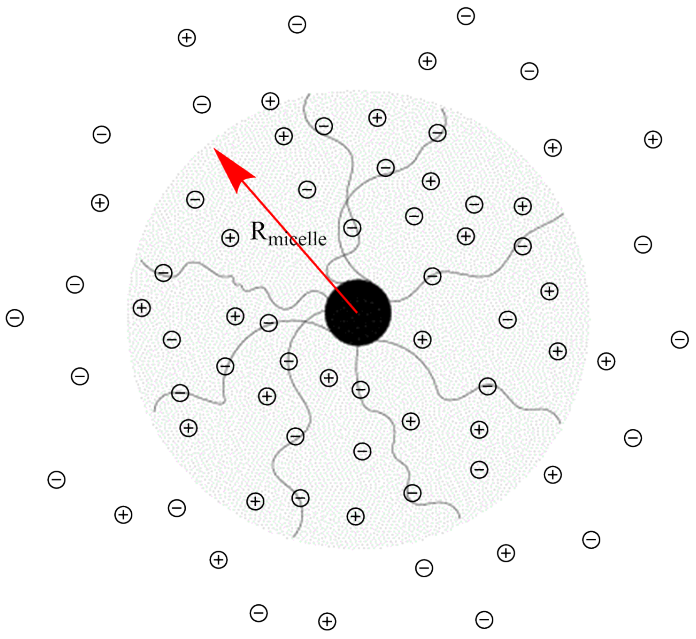

Figure 1.6: Schematic of a polyelectrolyte micelle, a spherical micelle with ionized corona and hydrophobic core in a solution of monovalent salt.

Micelle formation requires the presence of two opposing energies, i.e. an effective attrac-

tive force between the insoluble blocks, which leads to aggregation, and a repulsive force between the soluble blocks which hinders unlimited growth of the micelle into a distinct macroscopic phase. In other words, the association equilibrium and the structure of micelles formed by block copolymers with charged soluble blocks are represented by the opposition between hydrophobic attraction of insoluble blocks and the Coulomb repulsion between charged monomers in the micellar coronae. The latter interaction is unequivocally intervened by the counter-ions which are constantly there in the solution to guarantee its electro-neutrality all together. Micelles are stabilized in the solution due to the interaction of the soluble blocks and the solvent [4, 8].

1.3.2 Thermo-responsive amphiphilic block polymers

Temperature is the most manageable external stimulus that can be used to trigger solubility changes in thermo-responsive polymers upon both heating and cooling processes [12]. Temperature responsive polymers have drawn a lot of attention and have been applied in bioengineering and biotechnology [2]. Thermo-responsive polymers tend to go through major changes as a response to trivial alterations of temperature. Temperature is by far the most used stimulus for triggering a signal. It can be applied and control the temperature deviation from 37 °C under both the *in vitro* and *in vivo* conditions. This temperature deviation is used to stimulate the active release of therapeutic agents from various temperature-responsive drug delivery systems [45].

Lower Critical Solution Temperature (LCST)

The major feature of temperature-responsive copolymers is that by approaching their lower critical solution temperature (LCST), a stimulus can change the copolymer's hydration properties from being hydrophilic to hydrophobic, therefore the physicochemical properties are subjected to major changes [46].

LCST can be found in vast number of polymer solutions that are distinguished by well-built hydrogen bonds. Establishment of Hydrogen bonds between solutes and solvents decreases the total free energy of the solution; even so, the precise molecular orientations expected by means of these kinds of bonds causes negative entropy and positive free energy changes. This kind of phenomenon is very significant throughout aqueous media where the hydrophobic effect causes more negative entropy changes. Precipitation (coil-to-globule transition throughout very dilute media) in systems will occur above LCST, once the enthalpic influence on free energy is usually governed by growing entropic element from temperature ranges below the boiling point(Figure 1.7). Such systems

can be produced by adding hydrophobic segments to the water soluble polymer either by polymer modification or co-polymerization [18].

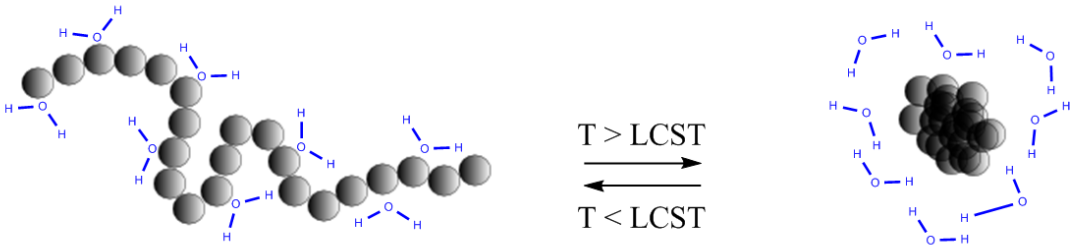

Figure 1.7: Coil to globule transition of an LCST linear homopolymer

Through LCST, the inter-molecular aggregations lead to intra-molecular collapse of individual polymer chains, which subsequently increases the scattering of light in solution (cloud point). As a result, by passing the cloud point, phase separation between the collapsed polymer molecules and the expelled water occurs [47]. To be able to observe the coil-to-globule transition for PNIPAAm it is important to work in very dilute solutions, otherwise the aggregation feature will dominate. Due to the fact that the thermo-responsive block in our block copolymer system is poly(N-isopropylacrylamide) (PNIPAAm), only the thermo-responsive systems based on PNIPAAm are reviewed in this part.

1.3.2.1 Poly(N-isopropylacrylamide) (PNIPAAm)

N-Isopropylacrylamide (NIPAM) is a temperature-responsive monomer that was first synthesized in the 1950s [45]. PNIPAAm is the most universally studied thermo-responsive polymer in aqueous mode [48]. It consists of a side group, a temperature sensitive conformation, and hydrogen bonding with water which is responsible for the water solubility of PNIPAAm. High molecular weight PNIPAAm exhibits LCST behavior at around 32 °C in water [12, 20, 48] and a couple of degrees lower in physiological saline solutions. The LCST of PNIPAAm strongly depends on both the molecular weight and concentration of the polymer in the low molecular weight range [21]. By increasing the solution temperature to above the transition temperature, a coil to globule transition will occur which is then followed by creation of aggregates and if the solution is not too dilute, macroscopic phase separation will happen. The transition temperature is called the cloud point (CP) [12]. It has been experimentally shown that high molar mass monodisperse PNIPAAm homo-

polymer chain in very dilute solutions, can fully collapse into a thermodynamically stable globule. It was shown for the first time that coil to globule transition is an irreversible process because there is hysteresis there [49, 50].

Applications

Roy and coworkers [6], have claimed in their recent review on thermo-responsive polymers that in spite of low toxicity of PNIPAAm (its trivial measured toxicity, is attributed to residual monomer), most of the PNIPAAm based materials that have been studied so far, are not examined for biocompatibility. Therefore, the application of these materials is limited to laboratory. Nevertheless, the applications of these thermo-responsive polymers in areas other than biomedical sciences would most probably become more significant.

1.3.2.2 PNIPAAm-based block copolymers

Combining PNIPAAm with other polymeric blocks will control the aggregation behavior of PNIPAAm. One way is to covalently add a water-soluble polymer such as poly(ethylene glycol) (PEG) to PNIPAAm that results in a double hydrophilic PNIPAAm-*b*-PEG copolymer at room temperature. The resulted diblock self-assembles into micelles with dehydrated PNIPAAm core and dissolved PEG corona at temperatures above the transition temperature [12].

Motokawa et al [51] have also synthesized the amphiphilic block copolymer, PNIPAAm-*b*-PEG with strong temperature-dependent solvent selectivity. The macroscopic observations (turbidity, fluidity and volume change) along with the microscopic observations (ultra-small and small-angle neutron scattering (USANS and SANS, respectively)) are an indication of various solution states. These states are happening due to the interplay of short-range interactions among PNIPAAm, PEG block chains, and solvent (especially temperature-dependent solvent selectivity) and long-range interactions arising from elastic energy of PNIPAAm and PEG in the domain structures.

PNIPAAm can also be grafted on a block copolymer and form a polymer comb. Yang et al [11] have synthesized mPEG-*b*-PA-*g*-PNIPAAm polymer combs. These copolymers self-assemble into spherical core-shell micelle aggregates with sizes below 200 nm which show a rather high LCST of 40 to 44.5 °C. They have shown that the physicochemical properties of the synthesized polymers depends on the lengths or molecular weights of the mPEG block and/or polymer compositions.

Hydrophobically-modified PNIPAAm-based block copolymers

Hydrophobic and hydrophilic segments in the polymeric chains have major impact on the LCST of a temperature responsive polymers. Normally, by randomly copolymerizing thermo-responsive polymers, PNIPAAm for instance, with a small ratio of hydrophilic monomers, the LCST will increase. In contrast, a small ratio of hydrophobic components was reported to decrease the LCST of NIPAAm while increasing its temperature sensitivity. More hydrophilic monomers such as acrylamide would make the LCST increase and even disappear, and more hydrophobic monomers such as N-butylacrylamide would induce the LCST to decrease [47].

In order to allow forming of nano-structures and also load them with drugs (hydrophobic ones for instance), it is mandatory to keep the PNIPAAm solution at elevated temperatures. Instead, to promote the self-assembly at lower temperatures, the PNIPAAm can be functionalized with hydrophobic residues such as octadecyl (C_{18}), or polystyrene (PS) groups which leads to C_{18}-PEG-C_{18} and PS-PEG-PS polymers, respectively. These systems form micelles with low stability and they are prone to phase separation. Suitable nano structures are formed when the amphiphilicity is tuned perfectly. One possibility to attain control of the self-assembly of PNIPAAm-based systems would be introducing a third polymer block, i.e., triblock terpolymer systems [12].

Shi and coworkers [52] have studied the solution behavior of hydrophobically modified PNIPAAm. The copolymer of NIPAAm and octadecylacrylate (ODA) was synthesized and its aggregation and phase separation have been studied. It has been shown that only a trivial amount of ODA can alter the amphiphilic properties of the polymer dramatically. The phase separation behavior has been observed at 30 °C which is lower than that of PNIPAAm itself.

In a recent work of Quan et al [12], non-ionic surfactant of PEG-octadecylether has been grafted to PNIPAAm and a series of end-capped *n*-octadecyl-PEG-*b*-PNIPAAm, have been synthesized. At low temperatures, they have detected well-defined micellar structures and by increasing the temperature up to near the LCST of PNIPAAm, the micelles collapse into smaller micelles at moderate temperatures, followed by inter-micellar aggregation and ultimately macroscopic phase separation occurs. SANS and SAXS data analysis recommend a coreshell structure for moderate temperatures. At elevated temperatures, the formed micelles shrink significantly which can be attributed to the collapse of PNIPAAm chains.

1.3.3 Charged thermo-responsive block copolymers

Micelles containing block polyelectrolytes, in other words, systems with a hydrophobic core and an ionic corona in aqueous media have been widely acknowledged and studied. The primary studies on these systems by Selb and Gallots was on micellization of PS-*b*-poly(4-vinylpyridinium) copolymers in water-methanol-Lbr mixtures. It was demonstrated that micelles show a star-like structure. The micellization process and micelle behavior were both discovered to be highly dependent on the solvent, temperature, salt concentration, and insoluble polystyrene block length [35].
Some block copolymers, contain more than one stimuli-responsive block which allows them to exhibit a more complex behavior. The stimuli-responsive blocks may be responsive to the same trigger, or to different ones. The polymer studied here is dual stimuli responsive, namely, thermo- and Ionic strength-responsive.
Masci and co workers have synthesized block copolymers of PNIPAAm and PAMPS with different block lengths. The LCST and the size of associations of these polymers are dependent on the relative block length and ionic strength. By increasing the size of the PAMPS block and decreasing the ionic strength, larger aggregates are formed which could be attributed to vesicles or micellar clusters [20].

LCST of charged thermo-responsive copolymers

Heyda and coworkers [46] have studied and analyzed the LCST dependence of charged thermoresponsive PNIPAAm based copolymers on their charge fraction and ionic strength by performing cloud-point experiments and theoretical analysis . The empirical and theoretical data are in good agreement and can be illustrated as Figure 1.8. They have established a thermodynamical model which relates the free energy (G) of a copolymer in a two-state, coil and globule, as a function of the specific volume.

1.4 Parameters influencing triblock terpolymer solution assembly

1.4.1 Effects of block sequence

The sequence of the different blocks in triblock copolymers (Figure 1.9) becomes very important because A-B-C, B-C-A, and C-A-B triblock copolymers are distinguishable and changing

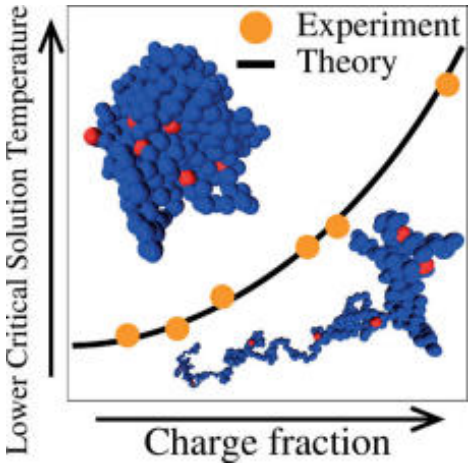

Figure 1.8: Lower Critical Solution Temperature (LCST) vs. Charge fraction

the block sequence leads to a change in the micellar morphology of triblock copolymers since they can influence the thermodynamic condition between midblock and endblocks [3].

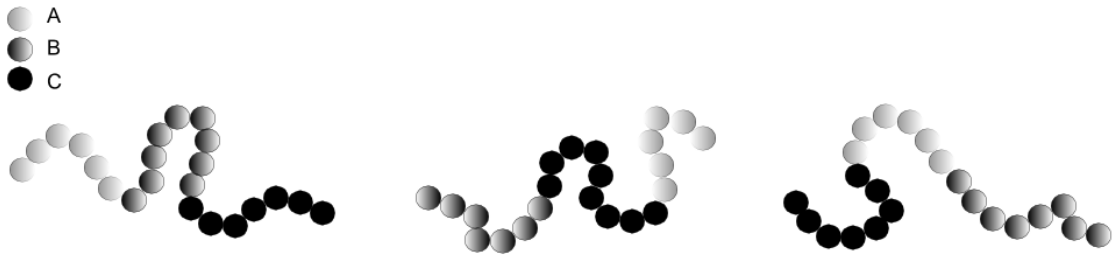

Figure 1.9: From left to right: A-B-C type, B-C-A type, and C-A-B type triblock copolymers.

Moreover, the sequence of blocks can affect the micellar diameters [3]. Zhang et al have empirically shown that PS-*b*-PEO-*b*-PAA and PEO-*b*-PS-*b*-PAA micelles are both different in morphology and diameter [53].

1.4.2 Effect of block lengths

Astafieva and co workers [35] have studied the effect of the insoluble block length on the CMC of block polyelectrolites and the CMC values for PS-*b*-PAN (poly(styrene)-*b*-poly(acrylonitrile)) copolymers have been measured. It was concluded that by increasing the insoluble block length,

the CMC values decrease drastically.

The aims and objectives of this thesis will be introduced in the following.

1.5 Master thesis aims and objectives

In this dissertation, the unique behavior of PNIPAAm containing amphiphilic block copolymers, together with their developing applications, encouraged us into studying a novel and rather complicated system. Nevertheless, there is not much publication about end-capped ABC triblock terpolymers. Moreover, being able to control the amphiphilicity will have a positive impact on the field of thermo-responsive polyelectrolyte micelles in various applications specially in drug delivery applications. That is why we mainly focused on characterizing a unique synthesized end-capped triblock terpolymer and studied its features in various conditions.

Aims

Owing to the promising features of the amphiphilic block copolymers and also thermo-responsive systems, it is interesting to study these systems more profoundly. It was therefore decided to focus on self-assembly of an end-capped thermo-responsive negatively charged triblock copolymer synthesized in our group by Dr. Kaizheng Zhu: n-octadecyl-poly(ethylene glycol)-poly(*N*-isopropylacrylamide)-*block*-poly(2-acrylamido- 2-methyl-1-propanesulfonic sodium), abbreviated as C_{18}-PEG_{10}-*b*-$PNIPAAm_{54}$-*b*-$PAMPS_{10}$ (Figure 1.10). The main aim of this study is to investigate the effects of temperature, polymer concentration and ionic strength on association properties of this amphiphilic triblock terpolymer in aqueous solutions with different ionic strengths.

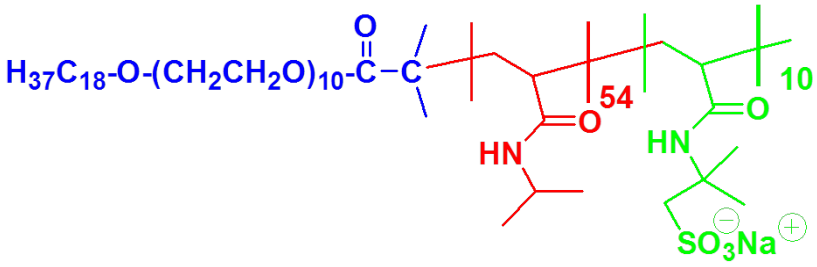

Figure 1.10: C_{18}-PEG_{10}-*b*-$PNIPAAm_{54}$-*b*-$PAMPS_{10}$

Objectives

The polymeric micelle associations have been prepared as a result of the self-assembly of the block copolymer in aqueous solutions with different ionic strengths. In the present work, effects of temperature, polymer concentration and salt addition have been studied through Dynamic Light Scattering (DLS), small angle neutron scattering (SANS), turbidimetry, densitometry, and zeta potential measurements. The molecular weights and molecular weight distributions of the copolymers have been determined by asymmetric flow field-flow fractionation (AFFFF) methods.
In the next chapter, the applied materials and methods are introduced (chapter 2). The results are presented and discussed in chapter 3. In the last chapter, the conclusion is presented together with some perspectives for further studies (chapter 4).

Chapter 2

Materials and methods

In this chapter, all experimental methods involved in fabrication and characterization of polymeric micelles are presented. Typical procedures and methods are reviewed: Synthesis of the studied charged LCST triblock terpolymer through the atom transfer radical polymerization (ATRP) method, and self-assembly of the polymeric micelles in aqueous solutions with different ionic strengths. We also detail and reference the materials, equipment and products which are commonly used for the experiments. Finally, we briefly present observation and characterization techniques: Zeta-potential experiment, Turbidimetry, Dynamic Light scattering (DLS), Densitometry, Small Angle Neutron Scattering (SANS).

2.1 Materials

2.1.1 Synthesis of C18-poly(*N*-isopropylacrylamide)-block-poly(2-acrylamido- 2-methyl-1-propanesulfonic sodium)

The triblock copolymer was prepared via ATRP procedure. $\mathrm{M_n}$ and PDI were measured by both $^1\mathrm{H}$ NMR and asymmetric flow field-flow fractionation AFFFF. The whole synthesis part and $\mathrm{M_n}$ and PDI measurements were performed by Dr. Kaizheng Zhu in the Polymer Group, Department of Chemistry, University of Oslo (UiO).

The molecular weight and polydispersity of the sample (Figure 2.1) was determined using Postnova software (AF2000 Control, version 1.1.011) with a Zimm-type fit. The number average molecular weight measured by AFFFF (2.8×10^4 g/mol) is higher than the structure determined by NMR would suggest (9.2×10^3 g/mol). This might be even though the AFFFF experiments were conducted at

a low temperature and a low polymer concentration, the formation of very small aggregates (di- or tri-mers) may interfere with the molecular weight determination.

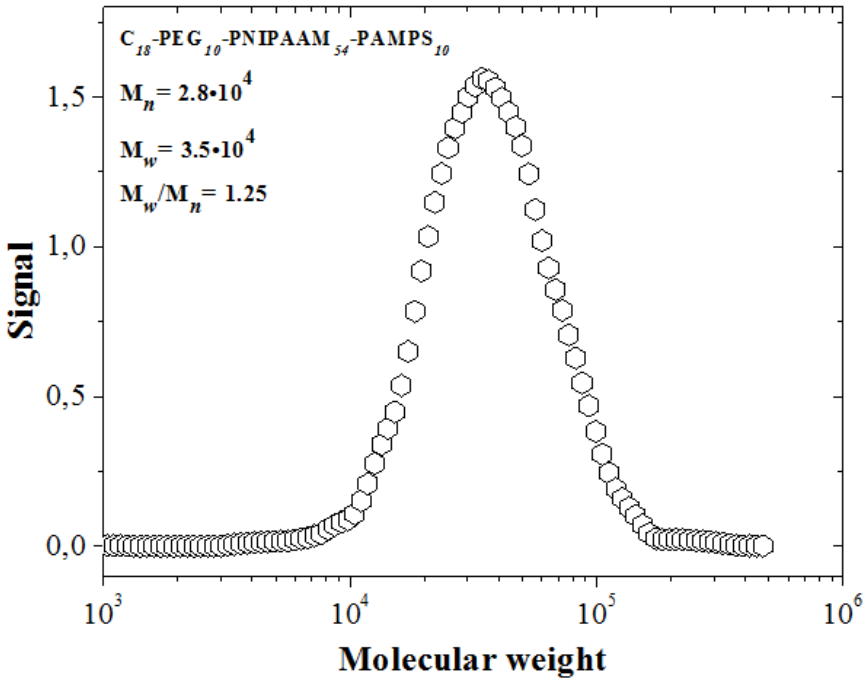

Figure 2.1: The molecular weight distribution curve of C_{18}-PEG_{10}-*b*-$PNIPAAm_{54}$-*b*-$PAMPS_{10}$ in dilute aqueous solution (0.1 M NaCl) at 5 °C by means of AFFFF.

2.1.2 Self-assembly of the polymer in aqueous solutions

For each sample, the proper amount of polymer, based on the desired concentration, was weighed and dissolved in millipore water at room temperature. The polymers were easily dissolved in water. The solutions were stirred for 24 hours to ensure the homogeneous solutions. There samples were afterwards kept in a refrigerator for another 24 hours and were thus prepared for measurements. In order to study the effect of salt addition to the polymer solutions, all samples were prepared in the same manner as for salt-free samples mentioned above, except that the solvent in this case was the NaCl solution in millipore water with the desired molarity. The association behavior of the polymer has been studied in water and four salt molarities: 0.05M, 0.1M, 0.5M and 1M. The salt solutions used for the experiments were prepared beforehand and the same solutions were used for making all samples and performing all experiments.

2.2 Methods

2.2.1 Zeta-potential experiment

Instrumentation and theory

Zeta potential (ζ) is an effective electrostatic potential at the electrical double layer surrounding a nanoparticle in colloidal dispersions. The stability of colloidal systems can be investigated through zeta potential measurements, and it is an indication of the degree of repulsion between similarly-charged adjacent particles. Nanoparticles with a zeta potential between -10 and +10 mV are considered to be more or less neutral, while nanoparticles with zeta potentials of higher than +30 mV or less than -30 mV are regarded as strongly cationic and strongly anionic, respectively. At these charge densities we consider the species to be electrostatically stabilized. A high zeta potential will present stability, so the solution will oppose aggregation. At the point when the potential is low, attraction surpasses repulsion and the particles will flocculate. Accordingly, micelles with high ζ potentials are stabilized electrically while micelles with lower ζ potentials have a tendency to aggregate [11, 54].

In an ionic solution, nanoparticles with a net charge are surrounded by a layer of oppositely charged ions. There is a tight bond between these ions and the surface of nanoparticles; this is referred to as the "Stern layer". There is also a second diffuse outer layer which is comprised of loosely associated ions. Stern layer together with the diffuse outer layer are identified as the electrical double layer. Due to the Brownian diffusion or applied force the particles move. By the particles moving, a distinction is created between ions in the diffuse layer that move along with the nanoparticle and ions that remain with the bulk dispersant. The electrostatic potential at this so called "slipping plane" boundary is called the zeta potential and is an indication of the surface charge of the nanoparticle. The employed instrumentation in this study is a Zeta-sizer Nano ZS instrument, Malvern instruments Ltd., United Kingdom. The sample cell that was used is a "dip" cell, including palladium electrodes with 2 mm spacing, one PCS1115 cuvette, and a cap. The instrument determines the electrophoretic mobility of the sample by the means of Laser Doppler Velocimetry (LDV) and calculates the zeta potential from such measurements on the basis of the Henry equation that relates the zeta potential, ζ, to the electrophoretic mobility, U_E (Equation 2.1)

$$U_E = \frac{2\varepsilon\zeta}{3\eta} f(Ka) \tag{2.1}$$

Where η and ε are the solvent's viscosity and the dielectric constant, respectively, at the given temperature. The Smoluchowski approximation to Henry's function ($f(Ka)$=1.5) was applied [54,

55].

Measurements

The experiments were carried out at a range of temperatures with closer intervals around the cloud point. The equilibrium time at each temperature was 150 seconds. The given zeta potential values in this study are the averages calculated on the basis of 3 runs both for a -68 mV standard and the sample.

2.2.2 Turbidimetry

Instrumentation and theory

Impact of temperature and temperature-dependence on the transmittance and cloud points of the solutions were determined via NK60-CPA cloud point analyzer from Phase Technology, Richmond, B.C., Canada. Utilizing this instrument, characteriziation of the phase changes of the sample is determined by scanning diffusive light scattering technique with high sensitivity and accuracy. A light beam with the peak wavelength of the employed AlGaAs light source at 654 nm, with a typical spectral half-width of 18 nm, is focused on the measuring sample. Directly above the sample there is an optical system with light-scattering detectors that unceasingly monitors the scattered intensity signal (S) of the sample while it is subjected to prescribed temperature alterations [21, 44, 56]. To transform the signal into turbidity, the relation between the calculated turbidity (τ) from the spectrophotometer experiments [56] and the signal (S) from the cloud point analyzer is found to be given by Equation 2.2 [56].

$$\tau(cm^{-1}) = 9.0 \times 10^{-9} S^{3.751} \tag{2.2}$$

Measurements

To perform the measurement, 0.15 mL of the test solution is employed by a micropipet onto a glass plate with a special design. This glass plate is coated with a thin metallic layer of very high reflectivity mirror. The sample surface is covered with 0.15 ml of highly transparent silicon oil in order to avoid evaporation of solvent at higher temperatures (needless to say, the density of the oil is lower than that of the sample). A platinum resistance thermometer probes the temperature of the sample, and a compact thermoelectric device (array of Peltier elements) located very close to the test solution is utilized to cool down and warm up the sample over a wide temperature range of

–60 to +60. The temperature can be changed very fast (up to 30 °C/min) and the cooling or heating rate can also be set to very low values. The instrument is connected to a PC, and the supplied software controls the operation of the turbidimeter and continuously collects data. In this work, the heating rate was set to 0.2 °C/min, and no effect of the heating rate on the signal was observed at low heating rates [56].
All data from the cloud point analyzer will be reported in terms of turbidity in this work (Equation 2.2). This powerful setup gives a remarkably high accuracy in the determination of the cloud point.

2.2.3 Dynamic Light scattering (DLS)

Instrumentation and theory

DLS experiments were conducted with the aid of a standard laboratory built Multi Angel Light Scattering (MALS) spectrometer with vertically polarized incident light which is supplied by an helium-ion laser with λ=632.5 nm). The beam is focused onto the sample cell through a temperature-controlled chamber.
In light scattering experiments we probe a wave vector $q = (4\pi n/\lambda)\sin(\theta/2)$, where λ is the wavelength of the incident light in a vacuum, θ is the scattering angle and n is the refractive index of the medium.
If the scattered field obeys Gaussian statistics (as for the present samples) the measured correlation function $g^2(q,t)$ can be related to the theoretically amenable first-order electric field correlation function $g^1(q,t)$ by the Siegert relationship $g^2(q,t) = 1 + B \mid g^1(q,t) \mid^2$, where B is an instrumental parameter. Experiment duration was 180s for each sample. Two relaxation modes can be described by Equation 2.3 called Kohlrausch-Williams-Watts (KWW) function.

$$g^1(q,t) = A_f \exp[-(\frac{1}{\tau_{fe}})^{\beta}] + A_s \exp[-(\frac{t}{\tau_{se}})^{\gamma}] \tag{2.3}$$

With $A_f + A_s = 1$. The parameters A_f and A_s are the amplitudes for the fast and slow relaxation mode, respectively. The variables τ_{fe} and τ_{se} are some effective relaxation times, and $\beta(0 < \beta \leq 1)$ and $\gamma(0 < \gamma \leq 1)$ and are the measure of the widths of the distributions of relaxation times. The width of the distribution decreases as the stretched exponent approaches 1. The mean relaxation times are given by Equation 2.4 and Equation 2.5 :

$$\tau_f = \frac{\tau_{fe}}{\beta}\Gamma(\frac{1}{\beta}) \tag{2.4}$$

$$\tau_s = \frac{\tau_{se}}{\gamma}\Gamma(\frac{1}{\gamma}) \tag{2.5}$$

Where $\Gamma(\beta^{-1)}$ and $\Gamma(\gamma^{-1})$ are the gamma functions of β^{-1} and γ^{-1} respectively. Analyses of the time correlation functions of the concentration fluctuations in the domain $qR_h < 1$ (R_h is the hydrodynamic radius) have shown that the short-time behavior is related to the mutual diffusion coefficient, D, ($\tau_f^{-1} = Dq^2$).

Since both modes are diffusive and we consider dilute solutions, the apparent hydrodynamic radius $\mathrm{R_h}$ (this is denoted R_{h_f}, and R_{h_s} (assuming that we have spheres)for the fast and the slow mode, respectively) is related to D via the Stokes-Einstein relationship: $D = \dfrac{k_B T}{6\pi\eta_0 R_h}$ Where k_B is the Boltzmann constant and η_0 is the viscosity of the solvent at temperature T [57].

In this study, the stretched exponential was not always the best fit and in many cases setting $A_f = 1$ sufficed to get a perfect fit with physically acceptable results.

Measurements

The very first step to perform a light scattering experiment is making a good that is a dust-free sample. Presence of dust in the samples will lead to a stronger scattering which gives us a wrong correlation function and a peak of high count-rate will be observed. In order to avoid dust, ca. 2ml of the samples is filtered in the light scattering tube inside a glovebox.

2.2.4 Densitometry

Instrumentation and theory

The lower critical solution temperatures (LCSTs) of the polymeric solutions were studied via densitometry. Solution density measurements were performed on a DMA5000 densitometer from Anton Paar, Graz. The densities are determined by an oscillating tube technique that exploits the relationship between the period of oscillation and density [22, 34, 58]. Tube containing fluid is oscillated at resonant frequency by electromagnetic vibrators. The resonant frequency, which is a function of the density of the fluid, is measured accurately. The tube is isolated from the fixtures by carefully designed bellows(Figure 2.2) [59].

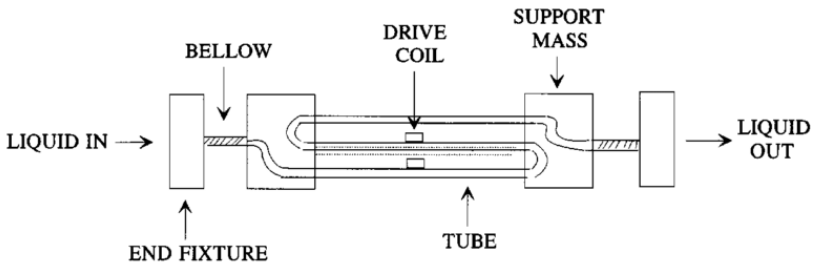

Figure 2.2: Schematic figure of oscillating tube densitometer

The relation holds when the viscosity of the sample is relatively low, as it is for the samples in the present work. The apparent partial specific volume, v_{solute}, of the solute is determined from the density measurements of a solution with solute and of the pure solvent as Equation 2.6:

$$v_{solute} = (\frac{1}{c_{solute}})(\frac{1}{d_{solute}}) - (\frac{1 - c_{solute}}{c_{solute}})(\frac{1}{d_{solvent}}) \tag{2.6}$$

where c_{solute} is the weight fraction of the solute, and d_{solute} and $d_{solvent}$ are the measured densities of the solution with the solute and of the pure solvent, respectively [22, 34, 58].

Another reason of performing density measurements is to calculate the specific volume of each block in order to use it in scattering length density (SLD) calculations which are later needed in SANS data analysis. If we have an n-block copolymer which their volume contributions is additive, the apparent specific volume of polymer can be calculated as Equation 2.7 where m_i is the mass fractions, and v_i is the specific volume of the ith blocks. Knowing the specific volume of each block provides an understanding about the behavior of the block polymer [58].

$$\bar{V} = v_{solute} = \sum_{i=1}^{n} m_i v_i \tag{2.7}$$

The density measurements were carried out in a temperature range from $5\,^{\circ}\mathrm{C}$ to $50\,^{\circ}\mathrm{C}$ in steps of $1\,^{\circ}\mathrm{C}$.

Measurements

The sample volume needed for density measurements is approximately 1.5 mL. Densities were measured for 0.5wt% polymer solutions. The densities were measured for the polymer solutions in water, 0.05M, 0.1M, 0.5M, and 1M NaCl solutions in steps of 1 degree from 5 to $50\,^{\circ}\mathrm{C}$. The densitometer was calibrated daily at $20\,^{\circ}\mathrm{C}$, using air and millipore water as reference samples.

In the temperature range from 20 °C to 50 °C the accuracy of the measurement is 0.000020 $\mathrm{g/cm^3}$, and it is 0.000050 $\mathrm{g/cm^3}$ from 55 to 90 °C. Because of the relatively low concentration of polymer, the derived apparent partial specific volumes have an accuracy of about 0.1-0.3% [34].

2.2.5 Small Angle Neutron Scattering (SANS)

Instrumentation and theory

Small angle neutron scattering (SANS) is a technique that can be employed to characterize nano-scale materials of the size range between 1 to 150 nm. Average size and distribution, spatial correlation of nano-scale structures, a long with the shape and internal structure of the particles are the extractable data from SANS measurements [60,61]. In light scattering, the investigation is performed on a wave vector (q) range of roughly 0.0005$\leq$ $q(\mathrm{\AA}^{-1})$ $\leq$0.005 however in SANS the system is probed in the range of 0.005$\leq$ $q(\mathrm{\AA}^{-1})$ $\leq$0.8, i.e. shorter length scales are probed. In accordance with the q-range, light scattering gives us a global overview of the system but in small angle scattering methods we will get information about the structures on local scales. Needless to say, the general equations and laws (for example, Guinier, Zimm, Kratky and Porod) are valid for any scattering technique. In SANS the samples are probed on the length scale of $2\pi/q$ which is a central quantity in the scattering experiments. The length scale (local or global scale) can be obtained from the inverse of the wave vector.

qL is a dimensionless quantity that is defined in scattering measurements. L is the characteristic length and is defined as R_g or R_h in dilute and ξ_s or ξ_D in semi-dilute regimes. When $qL < 1$ (Guinier region) scattered intensity is considered on a global dimension, while in the regime $qL \gg 1$ (fractal region), the inner structure of polymeric chains is observed.

Large increase in the scattering intensity at lower q is attributed to the existence of large aggregations. This upturn is usually described by a power-law equation with the power-law exponent being in the range of 2-4. Therefore in the fractal region, Equation 2.8 can be used to describe the scattered intensity.

$$I(q) \sim q^{-d_f} \tag{2.8}$$

where the d_f (fractal dimension which represents the local conformation of polymeric chains), is the slope of structure factor in the power law. For instance, d_f=3 shows a spherical or compact structure. For random coil in good and θ conditions d_f equals 1.7 and 2 respectively. d_f=1 is an indication of a rod-like conformation.

Data modeling

While the previously mentioned analysis are limiting laws, for a more detailed analysis of SANS results, we need to propose a structure for the aggregates which needs to be more complicated. The assumption of core-shell micelles was made and the data was modeled by core-shell form factor. This model can be written as Equation 2.10 for the assumed monodisperse star-like spherical entities.

Effective form factor $F(Q)$ holds all of the information of the shape and scattering contrast of the particle. The structure factor, $S(Q)$ explains the relative positions of the micelles in solution. In a dilute solution, the micelles do not interact with each other hence the $S(q) = 1$ for all the q values. In a more concentrated solution, this assumption is no longer valid [62]. The scattering length density (SLD) values of each block have been determined from the Equation 2.9.

$$\text{SLD} = \rho = \frac{\sum_{i=-1}^{n} b_{c_i}}{v_{solute}} \tag{2.9}$$

where b_{c_i} is the bound coherent scattering length of ith of n atoms in a molecule with molecular volume v_{solute} [63].

$$\begin{aligned} I(Q) = S(Q)\frac{\phi}{PV_{BCP}}(&\Delta\rho_{cp}^2 V_{cp^2} A(Q) c^2 + \\ &\Delta\rho_{sp}^2 P(P - F(0)_{blob}) V_{sp}^2 A(Q)_{sh}^2 + \\ &2\Delta\rho_{cp^2}\Delta\rho_{cp}^2 P^2 V_{PEO} V_{cp} A(Q)_c A(Q)_{sh} + \\ &V_{sp}^2 \Delta\rho_{sp}^2 F(Q)_{blob}(Q)) \end{aligned} \tag{2.10}$$

P is the aggregation number which is defined as the average number of chains per micelle, ϕ is the volume fraction, and $V_{BCP} = V_{cp} + V_{sp}$ is the overall molar volume of the block copolymer (V_{cp}) is the volume of C_{18} and V_{sp} is: $V_{PEG} + V_{PNIPAAm} + V_{PAMPS}$. The contrast which is determined by the scattering length density (SLD) difference between the polymer block (shell-forming polymer (i =sp) or core-forming polymer (i =cp)) and the solvent (i =0) would be $\Delta\rho_i = \rho_i - \rho_0$. [12]. Effective form factor, $F(Q)$ is calculated according to Equation 2.11.

$$F(Q) = \frac{P(Q)}{1 + \nu P(Q)} \tag{2.11}$$

where $P(Q)$ is the form factor of self-avoiding chains and ν is a parameter which increases with increasing concentration within the corona and is related to the chain-chain interaction within the corona [64].

Here the C_{18} is considered as the core which its scattering amplitude is calculated as Equation 2.12.

$$A(Q)_c = exp(-Q^2\sigma_{int}^2/2)\frac{3(\sin(QR_c) - qR_c\cos(QR_c))}{(QR_c)^3} \tag{2.12}$$

For the micellar shell the scattering amplitude is calculated according to equation 2.13.

$$A(Q)_{sh} = exp(-Q^2\sigma_{int}^2/2)\frac{1}{C}\int_{Rc}^{\infty} 4\pi r^2 n(r)\frac{\sin(Qr)}{Qr}dr \tag{2.13}$$

Here σ_{int} is the width of the core–corona interface and R_c is the radius of the core. $n(r)$ is a density profile for the corona for which we chose a flexible power-law profile multiplied with a cut-off function (Equation 2.14) [12].

$$n(r) = \frac{r^{-x}}{1 + exp((r - R_m)/\sigma_m R_m)} \tag{2.14}$$

Measurements

The SANS-instrument at the JEEP-II reactor of IFE at Kjeller, Norway was employed for the measurements. Liquid Nitrogen has been used to cool 15 cm long Be filter installed in the beam path in order to eliminate the fast neutrons (cutoff at a wavelength of $\lambda = 4$Å), and the extra 15 cm Bi filter is implemented to remove the γ radiation. The wavelength was set with the aid of a velocity selector (Dornier), using a high FWHM for the transmitted beam with a wavelength resolution ($\Delta\lambda/\lambda$) of 20%, and maximized flux on the sample. The neutron detector was a 128 $\times$ 128 pixel, 59 cm active diameter, ^{3}He -filled RISØ type detector, which is mounted on rails inside an evacuated detector chamber. The investigated scattering vector q-range was defined by the neutron wavelengths λ between 5.1 and 10.2 Å, and the sample-to-detector distance was adjusted from 1.0 to 3.4 m, covering the experimental q-range $8 \times 10^{-3} \leq q \leq 0.22$ Å^{-1}. The scattering vector q is given by $q = (4\pi n/\lambda)\sin(\theta/2)$, where θ is the scattering angle. In all the SANS measurements, deuterium oxide (D_2O) was used as a solvent instead of H_2O to attain a decent contrast and low background for the neutron-scattering experiments. All samples were inspected and shaken before being introduced into 5 mm quartz cuvettes. In order to have good thermal contact, the measuring cells were placed onto a copper-base and were mounted in the sample chamber. The detector chamber was evacuated to lessen the scattering caused from air. Standard reductions of the scattering data, including transmission corrections, were done by including data collected from empty cell, beam without cell, and blocked-beam background. The normalized scattered intensity can be calculated from direct beam measurements. Afterwards, these data were converted to an absolute scale (coherent differential cross section ($d\sum/d\Omega$)).

Chapter 3

Results and discussion

In this chapter the characteristics of neutral and saline aqueous solutions of C_{18}-PEG_{10}-*b*-$PNIPAAm_{54}$-*b*-$PAMPS_{10}$ that have been investigated will be discussed. The employed methods of characterization have been introduced in Chapter 2.

3.1 Zeta-potential measurements

Zeta-potential measurements are performed to determine the colloidal stability of the micelles. In general, the colloidal stability depends on the balance of Van der Waals attraction, electrostatic repulsion and steric forces [65]. Using a zeta-sizer instrument, the surface charge of the polymeric micelles at a range of temperature were determined and studied. These measurements were carried out on the dilute (0.1wt%) salt-free solution of the negatively charged block copolymer. The polymeric solution remained homogeneous through the whole measured temperature. The zeta-potential profile measurements of the micelles from 25 to 40 °C disclose temperature-induced response and micellar stability (Figure 3.1). The negative values are the result of the -SO_3^- functional groups of the charged block of PAMPS. By raising the medium temperature, the absolute values of the zeta potentials increase. It is known that at the elevated temperatures, micelles and inter-micellar aggregates press out the charges on the surface of the complexes. The observed increasing trend in the absolute values of the zeta potential of the nano-particles is consistent with the decreased micellar sizes by DLS measurements through the temperature (see 3.3). The rate of this increase gets higher by reaching the cloud point of the solution (see 3.2). This could be attributed to the collapsing of the PNIPAAm block [66]. By reaching the LCST, the coil to globule transition of the PNIPAAm block occurs which favors the stronger contraction and the contraction and pressing

out the charges is more efficient. Further increase in zeta potentials is due to the fact that the electrostatic repulsion and steric force are compensated by the Van der Waals force. The same behavior has been observed for positively charged PNIPAAm-containing diblock copolymers as well [14].

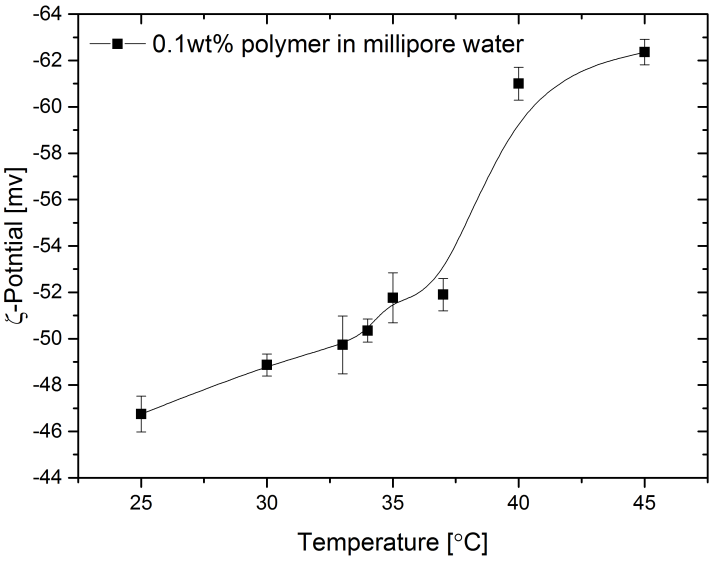

Figure 3.1: Plot of the Zeta potential versus temperature for 0.1 wt% solution of the block copolymers in millipore water

Other than the values for the zeta-potential, the Malvern device provides us with some complementary data which is an indication of the reliability of the data.
Unfortunately, it wasn't possible to measure the zeta-potentials for the dilute saline solutions since by increasing the ionic strength the conductivity increases and by exceeding the conductivity of c.a. 5 ms/cm, polarization and degradation of the dip cell's electrodes (due to movement of the conductive ions) will occur. Therefore, only the zeta-potential of the 0.1% solution in 0.05M NaCl at 25 °C was measured and the result is illustrated in Figure 3.2. The data collected from the zeta-potential measurements suggests a slightly lower zeta-potential for the sample in the 0.05M solution which could be attributed the screening of the negative surface charges performed by the solvent.
The quality of data can be evaluated by scrutinizing some additional data that can be extracted from the device. The zeta-potential distribution diagram portrayed in Figure 3.3 shows a typical measurement with good quality.

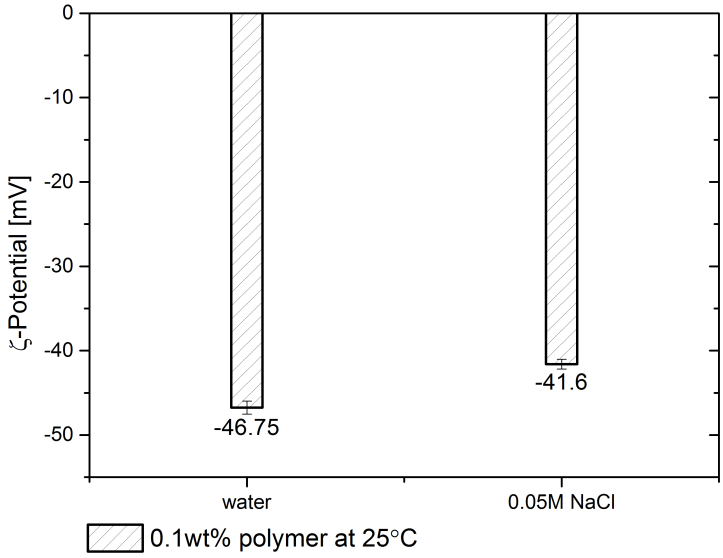

Figure 3.2: Zeta potential of 0.1 wt% solutions of the block copolymers in millipore water and 0.05M NaCl at 25 °C

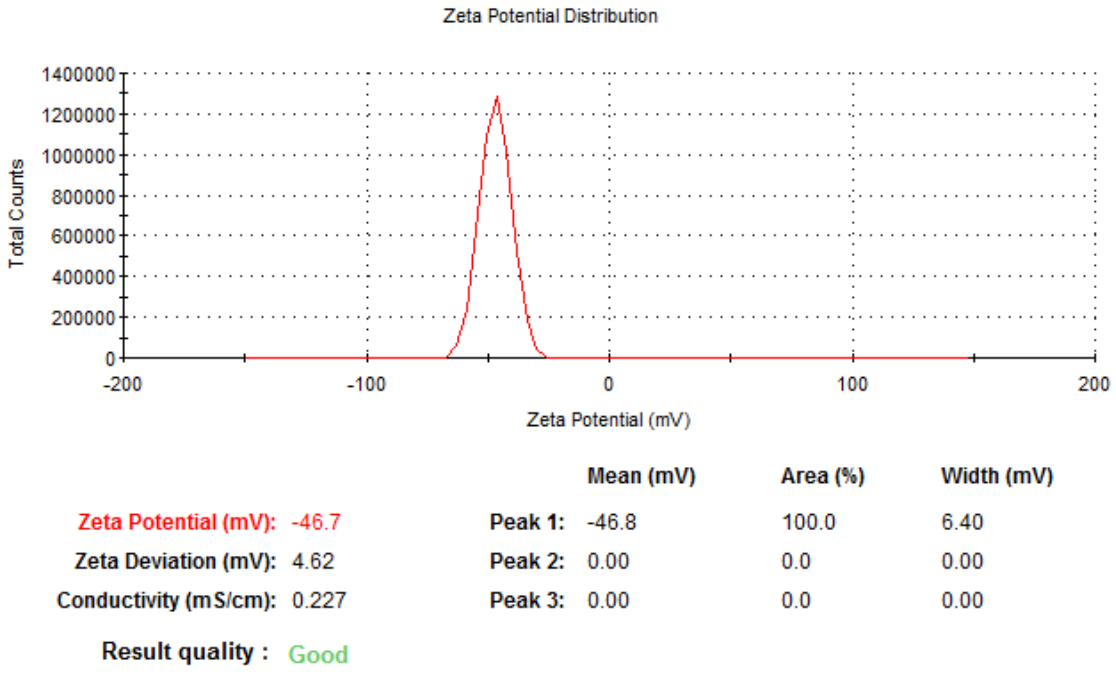

Figure 3.3: Zeta potential distribution of the 0.1 wt% solution of the block copolymer in millipore water at 25 °C with good result quality

A 'good' phase plot is characterized by each of the sections being clearly identifiable, consistent and symmetric and with little or no noise. Figure 3.4 demonstrates a high quality phase data from a zeta potential measurement. This displays the phase shift that occurs during the Zeta measurement. The circled region is the fast and the "V" shaped curve is the slow field reversal region of the measurement. Data from the first (circled) part of the phase plot determines the mean zeta potential value and it should be rapidly oscillating around lower voltages[1].

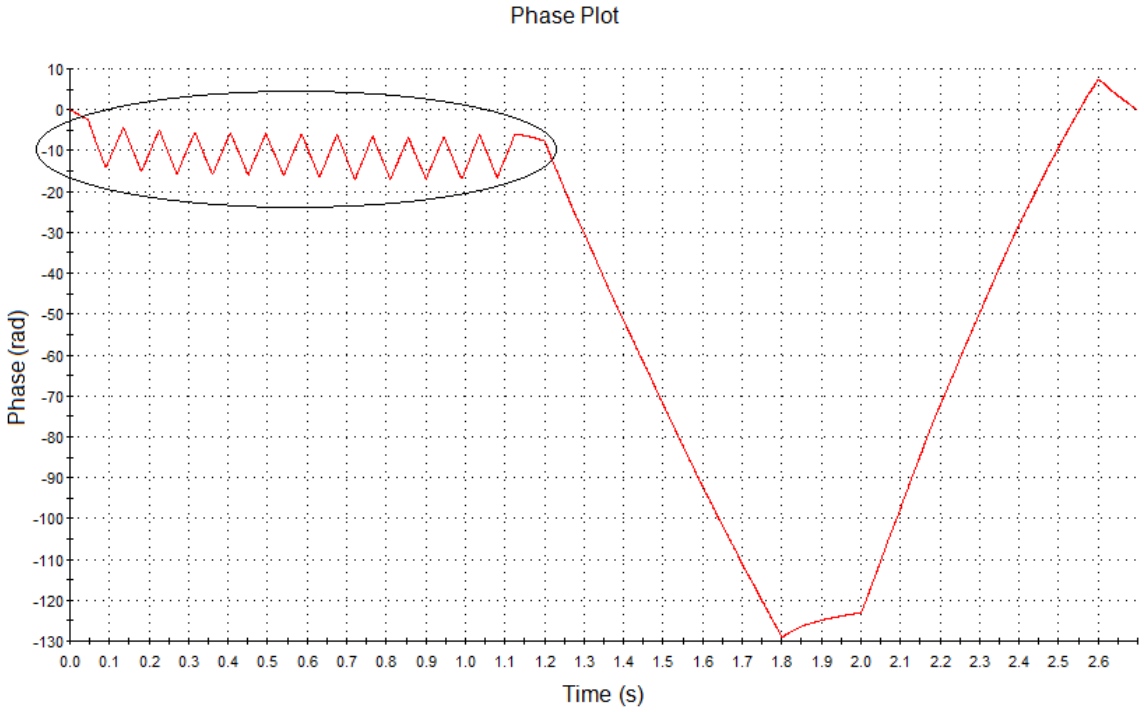

Figure 3.4: Phase plot of the 0.1 wt% solution of the block copolymer in millipore water at 25 °C with good result quality

3.2 Turbidimetry

A distinctive feature of a thermo-responsive block copolymer is that by going above its transition temperature, its turbidity undergoes major changes which is referred to as cloud point (CP). The studied block copolymer here, demonstrates LCST behavior, which means that the solutions tend to phase separate at elevated temperatures. What happens here is that the hydrophobic

[1]To interpret the 'zeta-potential distribution diagram' and the 'phase plot', we relied on the help of the Malvern Zetasizer Software 6.20, Copyright ©2002-2010 Malvern Instruments Ltd.

associations among the micelles grow and the micelles become less soluble.

Quan et al [12] have performed turbidity measurements on PNIPAAm homopolymer, C_{18}-PNIPAAm, and C_{18}-PEG-PNIPAAm. They have shown that PNIPAAm exhibits a sharp transition to a turbid solution at the approximate temperature of 34–35 °C. For the end-capped C_{18}-PNIPAAm, even at lower temperatures the intrinsic values of turbidity are higher. The shift of the cloud point is observed at 32 °C. For the C_{18}-PEG-PNIPAAm copolymers (with different lengths of PEG), the cloud point is shifted to the temperature of about 40 °C due to the increased solubility of PEG and formation of more stable micelles.

Our block copolymer's behavior have been studied both in water and saline solutions through temperature. Generally, intensification of the turbidity with increasing temperature, reveals the formation of inter-micellar structures. When the PNIPAAm block is long enough in the polymer chain, the PNIPAAm segments contract to avoid water exposure [67]. Adding salt increases the ionic strength in a polymeric solution. As a result, the surfaces charges of the micelles will be screened out and due to the repulsive forces which hindered aggregation, are weakened or removed (depending on the ionic strength) and aggregation of micelles happen at lower temperatures.

The temperature dependencies of the turbidity for 0.5wt% polymer solutions with different salt concentrations is illustrated in Figure 3.5. It can be perceived that the transition in turbidity is shifted towards lower temperatures as the salt concentration increases. However, the turbidity becomes less pronounced. The reason for this strange turbidity behavior at high salinity with lower values at higher temperatures is probably due to accumulation of polymer onto the mirror surface (multiple layer).

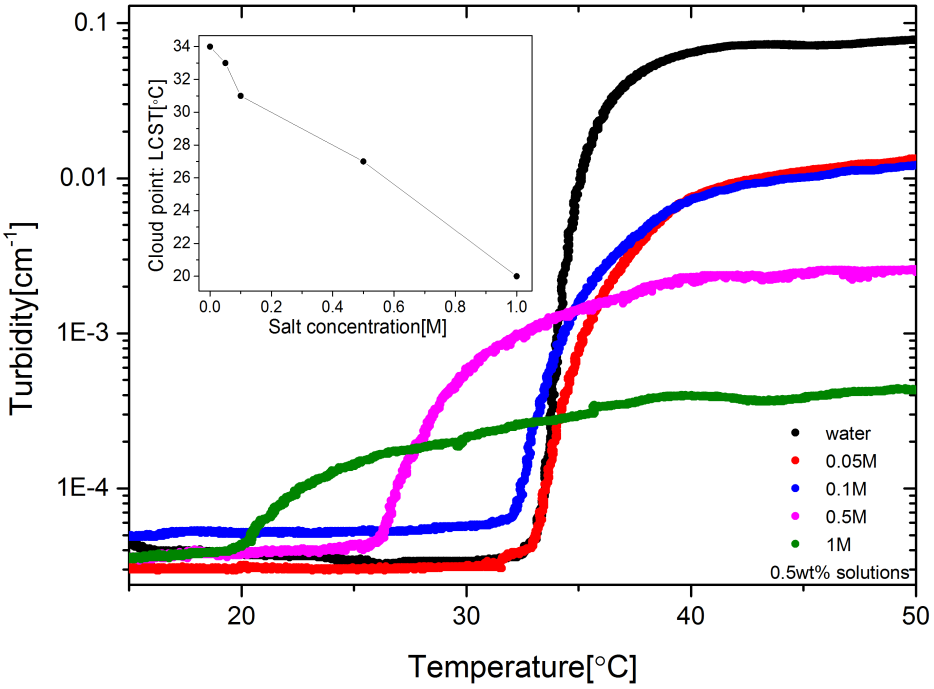

Figure 3.5: Turbidity vs. temperature for 0.5wt% solutions of C_{18}-PEG_{10}-*b*-$PNIPAAm_{54}$-*b*-$PAMPS_{10}$ at different ionic strengths.

By increasing the temperature above the CP and the consequent growth of the hydrophobic segments, macroscopic phase separation occurs and the turbidity amounts above the CP remain almost the same after a certain temperature. Aggregation and contraction are two processes that are happening simultaneously. At lower temperatures the aggregation of micelles is more dominant, while at higher temperatures the opposite trend is observed. The screening effect of the electrostatic interactions will be more prominent as the ionic strength is increased. Although the general behavior of the turbidity will remain the same for all kinds of ionic strengths, addition of salt however leads to a depression of the cloud point. This could be attributed to the gradual screening of the electrostatic interactions as the salinity of the solution increases. This results in more sticky particles at lower temperatures, and thereby this process facilitates growth of aggregates at lower temperatures [44]. Figure 3.6 shows 1wt% samples in different salt concentrations at three temperatures. The photos have been taken right after taking the samples out of the fridge (5 °C), at room temperature (25 °C) and at 40 °C.

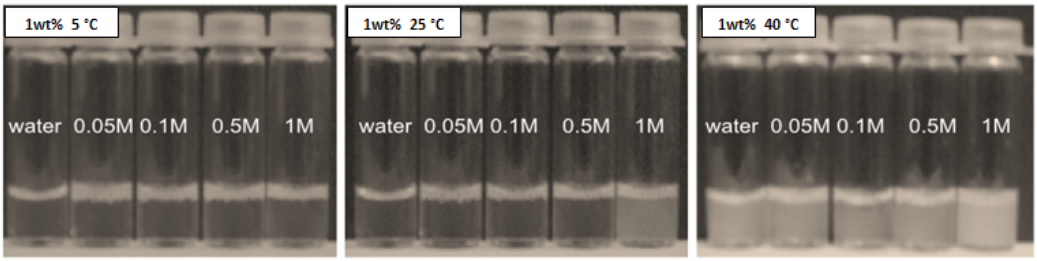

Figure 3.6: 1wt% solutions of C_{18}-PEG_{10}-*b*-$PNIPAAm_{54}$-*b*-$PAMPS_{10}$ in water, 0.05M NaCl, 0.1M NaCl, 0.5M NaCl, and 1M NaCl at different temperatures.

Effect of concentration on the turbidity of the solutions has been studied as well. Figure 3.7 shows 0.1wt%, 0.3wt%, 0.5wt%, 0.7wt% and 1wt% salt-free polymer solutions at 5 °C, 25 °C) and 40 °C. As a general trend and as it is illustrated in Figure 3.8, by increasing the polymer concentration the cloud point is shifted to lower temperatures. Nevertheless, the turbidity appears to be more prominent as the polymer concentration rises. The upturn of the turbidity is much stronger for higher polymer concentrations which is an indication that unimers form micelles and intermicellar structures. Above the cloud point, as the increase in hydrophobicity of the polymer happens, they become sticky, and this leads to the formation of intermicellar complexes. By increasing the polymer concentration the collision frequency of the polymeric groups will increase and resulting in larger aggregates.

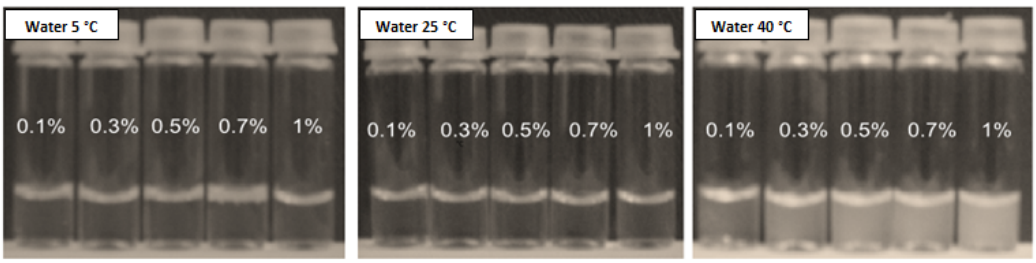

Figure 3.7: 0.1wt%, 0.3wt%, 0.5wt%, 0.7wt% and 1wt% solutions of C_{18}-PEG_{10}-*b*-$PNIPAAm_{54}$-*b*-$PAMPS_{10}$ in water at different tempetarures.

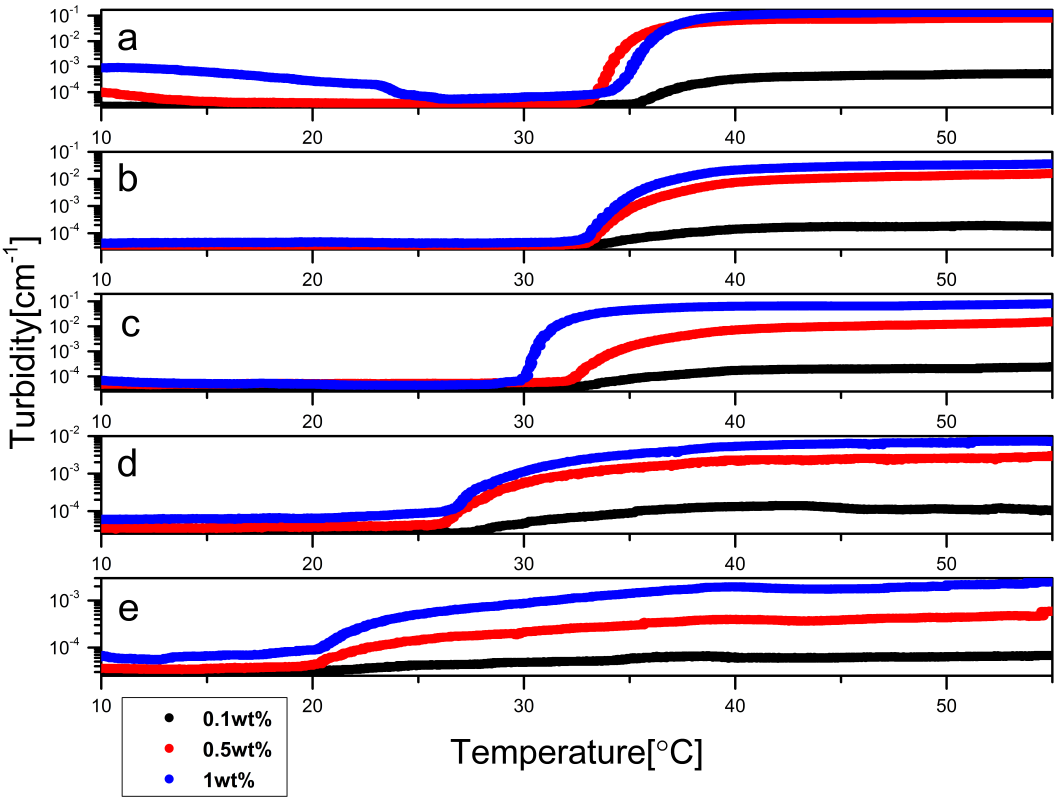

Figure 3.8: Turbidity vs. temperature for 0.1wt%, 0.5wt% and 1wt% solutions of C_{18}-PEG_{10}-*b*-$PNIPAAm_{54}$-*b*-$PAMPS_{10}$ in a) water, b) 0.05M NaCl, c) 0.1M NaCl, d) 0.5M NaCl, and e) 1M NaCl.

Flory-Huggins interaction parameter χ_{eff} is a function of temperature and concentration. This parameter will gain higher values as the temperature and polymer concentration are increased which is an indication of poor thermodynamical conditions hence the aggregates will be formed [21].

3.3 Dynamic light scattering (DLS)

Hydrodynamic radii of the micelles and their temperature and ionic strength dependencies were investigated by multi-angle dynamic light scattering (DLS). The homodyne intensity autocorrelation function $g^2(t)$ was measured simultaneously in 8 angles starting with θ=22 ° and 17 ° intervals, however, not all the angles were used for analyzing (the correlation functions of the selected

angles are illustrated in Figure 3.11). Equation 2.3 was employed in the analysis.

In order to consider the temperature-induced changes in solvent viscosity, the first-order electric field autocorrelation function, $g^{(1)}(t)$, at the scattering angle of 107 ° is plotted against tT/η_0 (t is the time, T is the solution temperature, and η_0 is the solvent viscosity) for the 0.5wt% solutions at various temperatures both in salt-free water (Figure 3.9) and water with added salt (Figure 3.10).

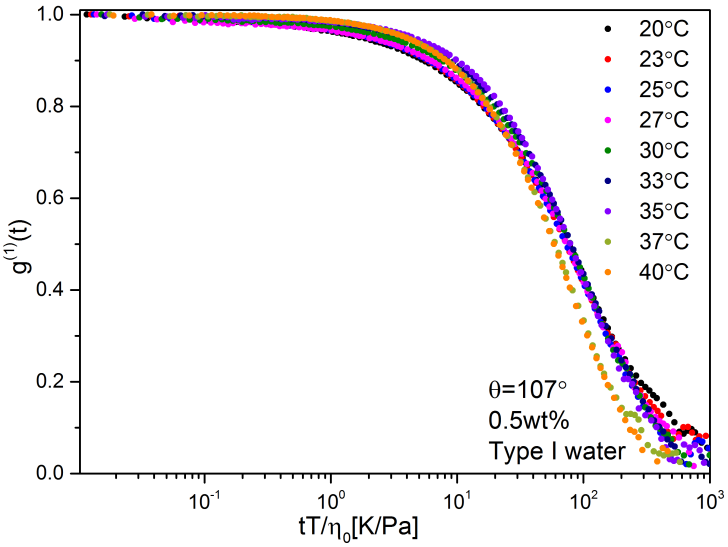

Figure 3.9: First-order electric field autocorrelation function vs. tT/η_0 for 0.5wt% solution of C_{18}-PEG_{10}-*b*-$PNIPAAm_{54}$-*b*-$PAMPS_{10}$ in type I water at the scattering angle of 107 °

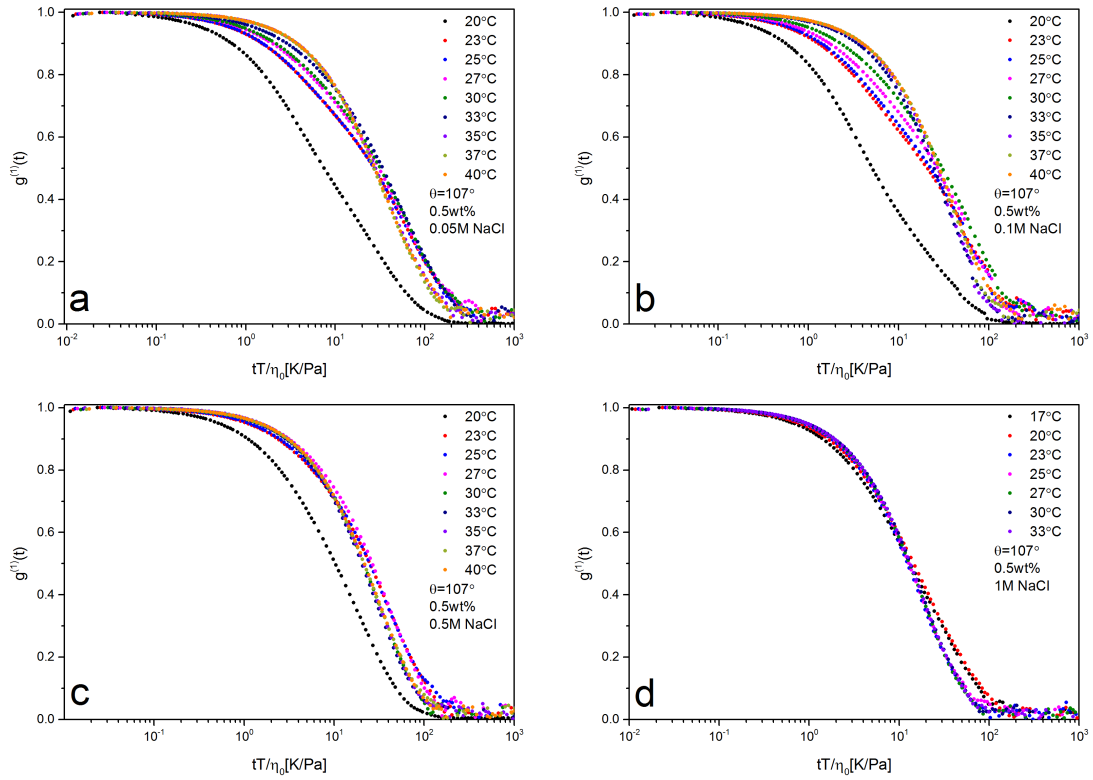

Figure 3.10: First-order electric field autocorrelation function vs. tT/η_0 for 0.5wt% solutions of C_{18}-PEG_{10}-*b*-$PNIPAAm_{54}$-*b*-$PAMPS_{10}$ in a) 0.05M, b) 0.1M, c) 0.5M, and d) 1M NaCl at the scattering angle of 107 °

As a general trend, the correlation of the signal takes longer time to decay for larger particles. Small particles on the other hand, move more rapidly so the correlation signal tends to decreases more quickly.

By analyzing the time correlation functions in this study, it was perceived that the first and the second term (when applicable) in equation 2.3 are both related to the mutual diffusion coefficient (*D*) the equation ($\tau_f^{-1} = Dq^2$). This q^2-dependence discloses the diffusivity of the system [56]. The curves in Figure 3.11, shown for 0.5wt% solutions in water at 2 different temperatures, are almost covering each other at given angles (only the angles are shown that have been used for analyzing the DLS data). In some cases such as Figure 3.11a, a slight deviation of curves has been considered as an instrumental error.

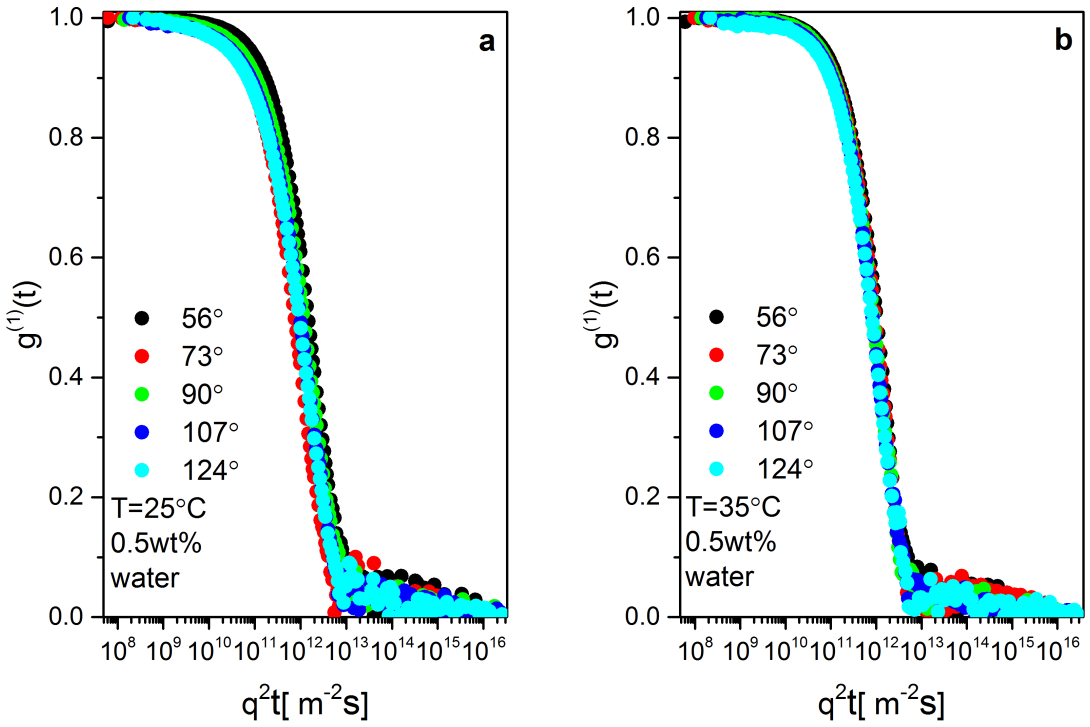

Figure 3.11: First-order electric field autocorrelation function vs. q^2t for 0.5wt% solutions of C_{18}-PEG_{10}-*b*-$PNIPAAm_{54}$-*b*-$PAMPS_{10}$ at a) 25 °C and b) 35 °C at different scattering angles in Type I water

In Figure 3.12 the correlation functions and their corresponding fits of 0.5wt% C_{18}-PEG_{10}-*b*-$PNIPAAm_{54}$-*b*-$PAMPS_{10}$ in water at 25 °C are plotted. The relaxation times (τ values) are extracted from the unimodal fits for each correlation function (different q values). The inset plot illustrates the inverse values of relaxation times plotted against q^2. The slope of this plot represents the apparent diffusion coefficient *D*, which in diffusive systems is not dependent on the scattering angle. The inverse relaxation time is q^2 depended, and this is the hallmark of a diffusive process.

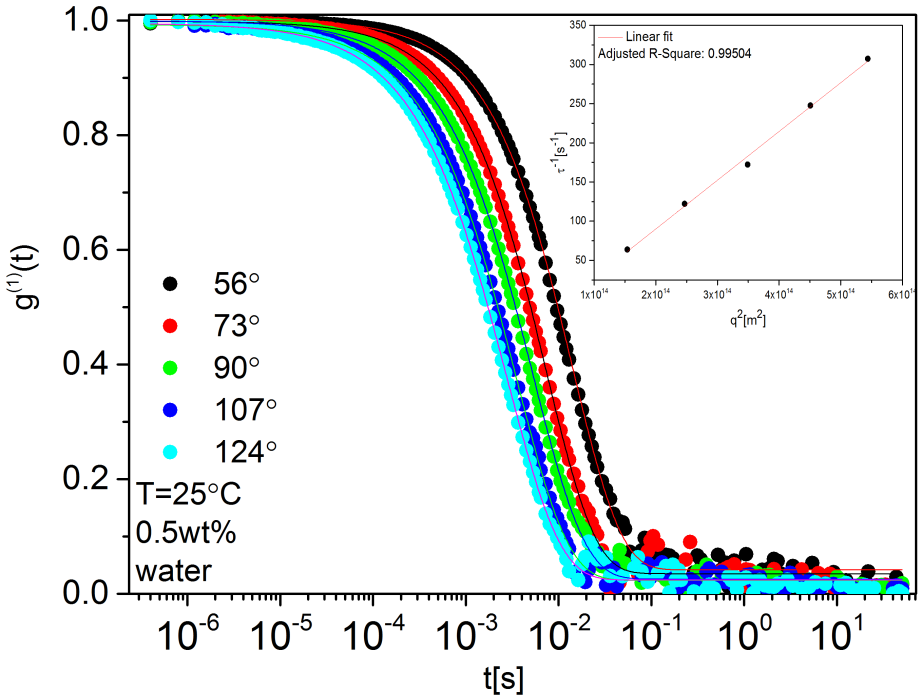

Figure 3.12: First-order electric field autocorrelation functions and their corresponding fits of 0.5wt% C_{18}-PEG_{10}-*b*-$PNIPAAm_{54}$-*b*-$PAMPS_{10}$ in water at 25 °C

In order to demonstrate the precision of the fits, the decay of the correlation function for the angle 107 ° together with its single exponential fit is plotted separately in Figure 3.13. The inset plot illustrates the random distribution and small values of the residuals which is showing a good agreement between the correlation function and its respective fit.

The same trend is observed in Figure 3.13 and Figure 3.14 for the same sample only at the higher temperature of 35 °C.

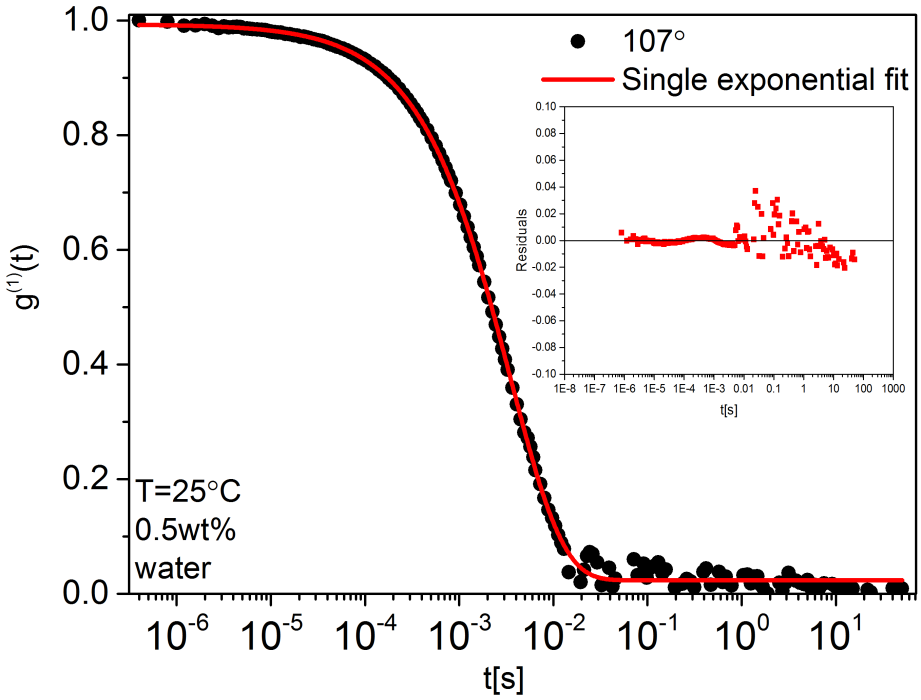

Figure 3.13: First-order electric field autocorrelation function and its corresponding fit at 107 ° of 0.5wt% C_{18}-PEG_{10}-*b*-$PNIPAAm_{54}$-*b*-$PAMPS_{10}$ in water at 25 °C

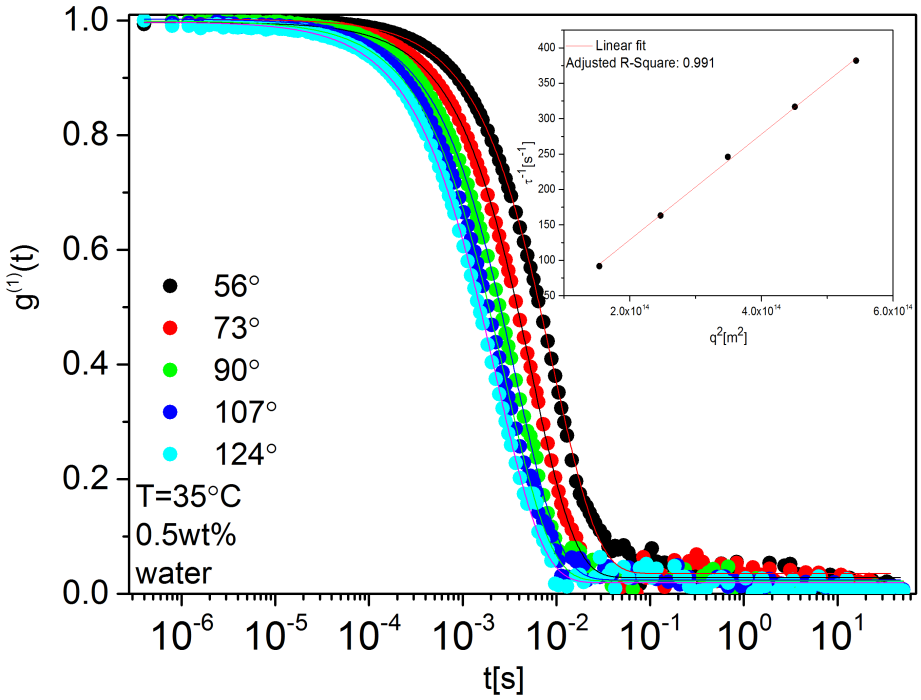

Figure 3.14: First-order electric field autocorrelation functions and their corresponding fits of 0.5wt% C_{18}-PEG_{10}-*b*-$PNIPAAm_{54}$-*b*-$PAMPS_{10}$ in water at 35 °C

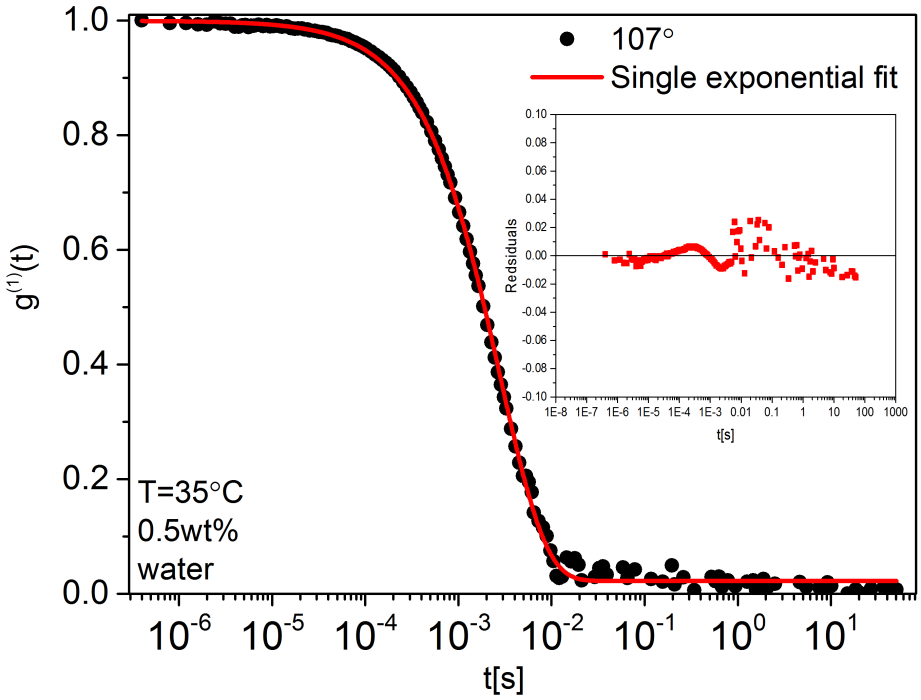

Figure 3.15: First-order electric field autocorrelation function and its corresponding fit at 107 ° of 0.5wt% C_{18}-PEG_{10}-*b*-$PNIPAAm_{54}$-*b*-$PAMPS_{10}$ in water at 35 °C

All the samples showed a mono-disperse behavior at all the temperatures except for two. The decay of the correlation functions for 0.5wt% C_{18}-PEG_{10}-*b*-$PNIPAAm_{54}$-*b*-$PAMPS_{10}$ at 17 and 20 °C exhibited bimodal behaviors. According to the turbidity measurements, this kind of behavior happened bellow the CP. In figure 3.16 the correlation functions and their corresponding fits of 0.5wt% C_{18}-PEG_{10}-*b*-$PNIPAAm_{54}$-*b*-$PAMPS_{10}$ in 1M NaCl at 20 °C are illustrated. The diffusion coefficient for both of the fast and slow modes are deduced from the inset plots. Clearly, the bimodal fit has been a better choice.

Figure 3.17 the correlation function and its respective fit at 107 ° is shown. The corresponding residuals for both single and double exponential fits are shown simultaneously in the inset plot. Clearly, the bimodal fit is demonstrating better residuals. In bimodal correlation functions (systems with two relaxation modes), the diffusion coefficient for the slower mode (larger hydrodynamic radius) has a smaller value than the diffusion coefficient for faster mode (smaller hydrodynamic radius).

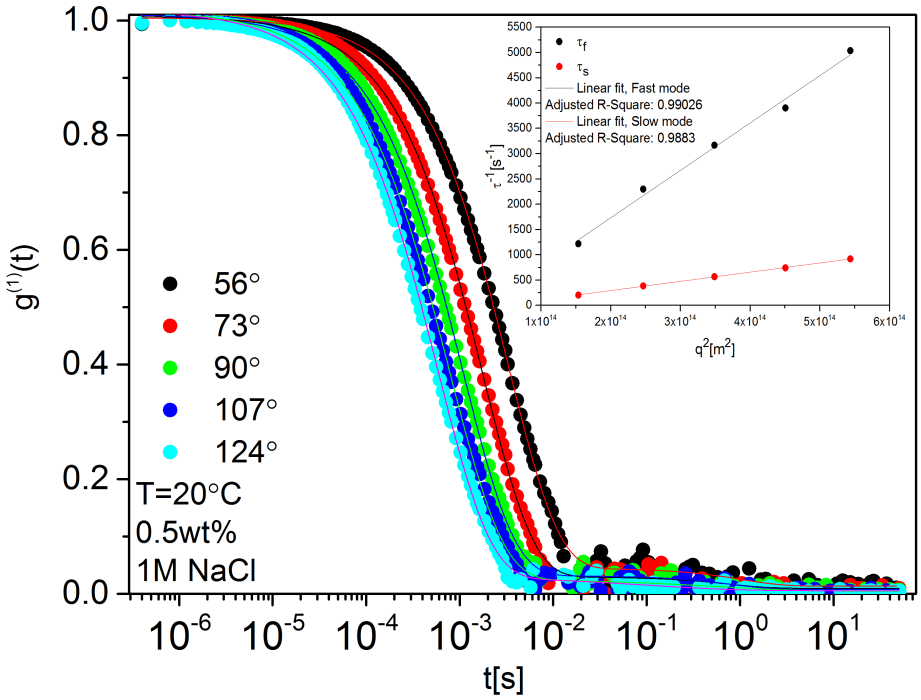

Figure 3.16: First-order electric field autocorrelation functions and their corresponding fits of 0.5wt% C_{18}-PEG_{10}-*b*-$PNIPAAm_{54}$-*b*-$PAMPS_{10}$ in 1M NaCl at 20 °C

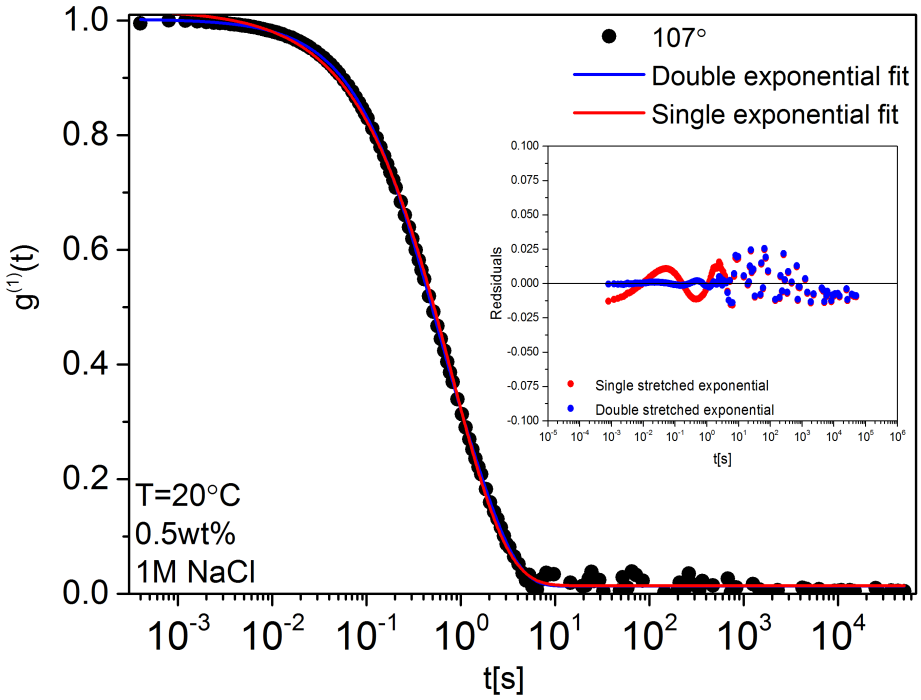

Figure 3.17: First-order electric field autocorrelation function and its corresponding fit at 107 ° of 0.5wt% C_{18}-PEG_{10}-*b*-$PNIPAAm_{54}$-*b*-$PAMPS_{10}$ in 1M NaCl at 20 °C

The hydrodynamic radii and their corresponding beta values of all the samples are plotted against temperature (Figure 3.18, 3.19, 3.20, 3.21, 3.22, lines in the figures are for visibility only). Generally, the micelles tend to grow in size and form aggregates by increasing the temperature up to approximately the cloud points obtained from the turbidity measurements. Subsequently the sizes were decreased which is an indication of collapsing and contracting of the PNIPAAm block due to its LCST behavior. At the same time, the β values are increasing as the temperature rises which reflects an increasing width of the distribution of relaxation times by temperature. The distribution of relaxation times becomes narrower at higher temperatures, and β approaches its ultimate value of 1 which suggests that developed complexes are formed at elevated temperatures and are almost of the same size. The β values are calculated mean values with the maximum standard deviation of ± 0.02 for each temperature but in order to avoid chaos in the plots, no error bars have been added.

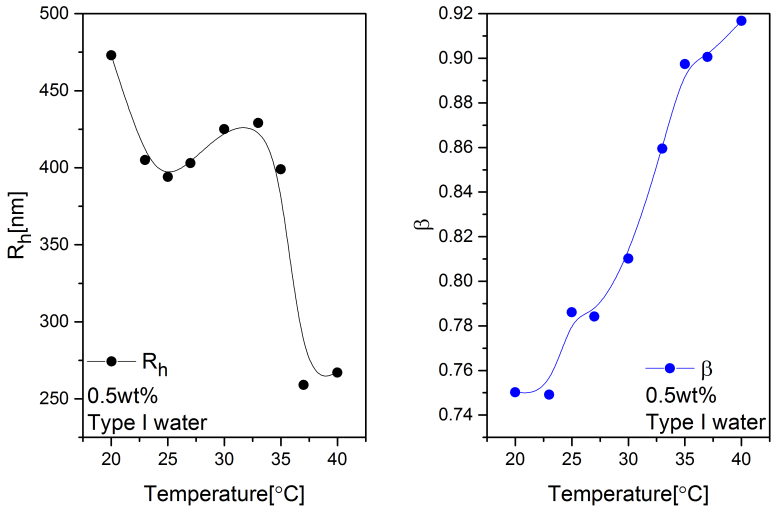

Figure 3.18: Hydrodynamic radii and beta values vs. temperature for 0.5wt% samples in water

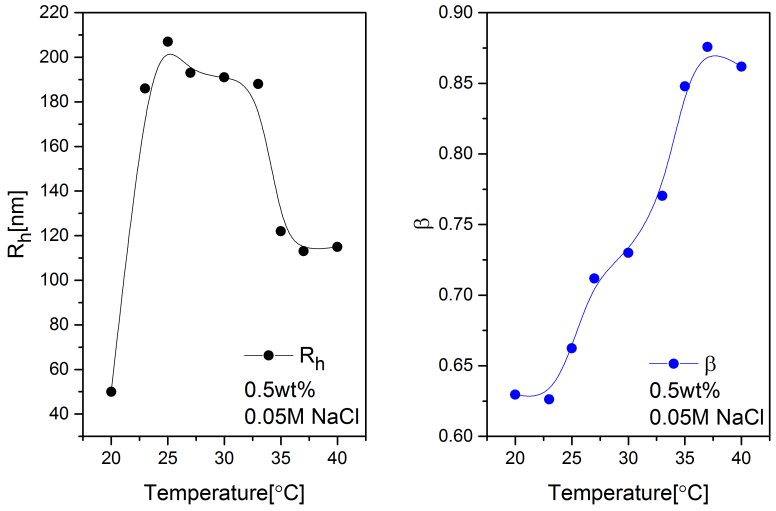

Figure 3.19: Hydrodynamic radii and beta values vs. temperature for 0.5wt% samples in 0.05M NaCl

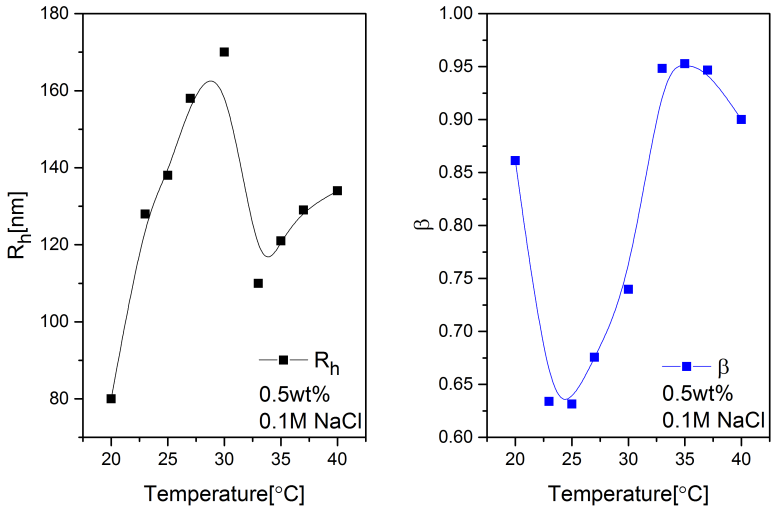

Figure 3.20: Hydrodynamic radii and beta values vs. temperature for 0.5wt% samples in 0.1M NaCl

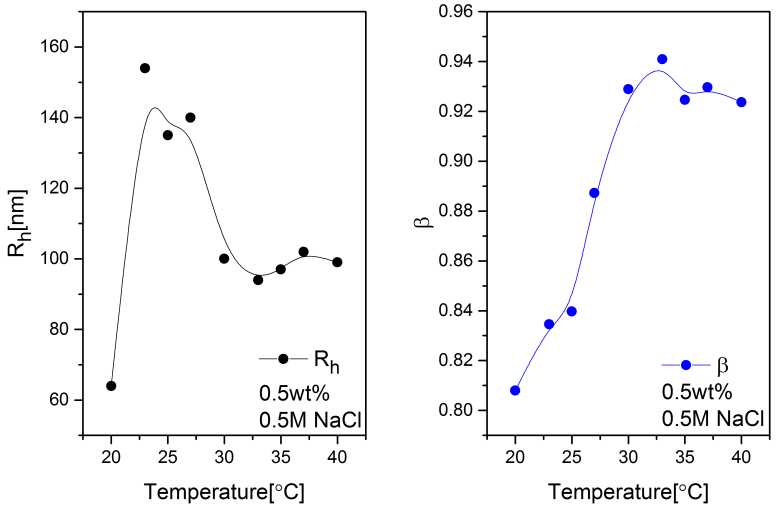

Figure 3.21: Hydrodynamic radii and beta values vs. temperature for 0.5wt% samples in 0.5M NaCl

Since the CP of the solutions in 1M NaCl happened at around 20 °C (according to the turbidity measurements), the sample was also measured before this temperature at 17 °C (Figure 3.22). It wasn't also possible to continue the measurements up to 40 °C due to macroscopic phase separation of the sample. It is interesting that below the CP, the solution is completely poly-disperse but by increasing the temperature, aggregation occurs and mono-disperse clusters are formed.

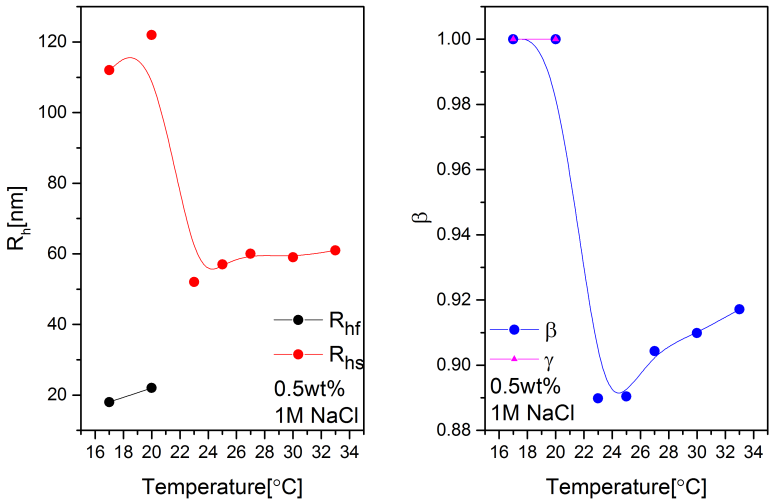

Figure 3.22: Hydrodynamic radii and beta values vs. temperature for 0.5wt% samples in 1M NaCl

The previous figures are summarized in Figure 3.23. It can be perceived that increase in the ionic-strength results in the more compact copolymer aggregates. Screening of the charges due to salt addition leads to a more hydrophobic structure which has higher mobility. It is evident at low temperatures that salt addition leads to compression of the species as a consequence of the progressive screening of the electrostatic interactions. Further temperature raise facilitates the breakage of hydrogen bonds and the species become stickier, which results in growth of aggregates and higher values of R_h. At high salt concentrations, on the other hand, the high sticking probability favors aggregation.

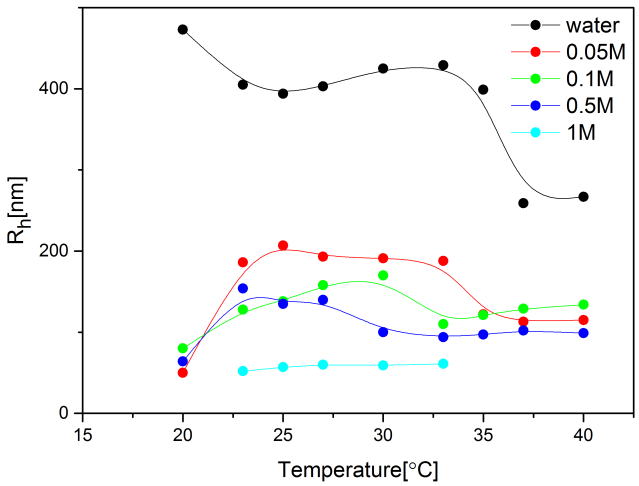

Figure 3.23: Hydrodynamic radii vs. temperature for 0.5wt% samples

3.4 Densitometry

The apparent specific volume of C_{18}-*b*-PEG_{10}-*b*-$PNIPAAm_{54}$-*b*-$PAMPS_{10}$ in the micellar state as a function of temperature has been determined utilizing a highly precise densitometer DMA 5000 from Anton Paar in a temperature range of 5 to 50 °C (Figure 3.24).

For all the samples an increase in the specific volume is detected with increasing temperatures. This trend has also been observed for the octadecyl in the micellar state, and PEO both in the micellar state and the form of homopolymer [58] which is consistent with the increase in thermal motion. The sample with the highest ionic strength has the lowest specific volume i.e. it has the highest specific density. It could be attributed to the salt screening effect. By screening the charges due to the presence of salt ions, the electrostatic repulsions will diminish and polymer chains tend to collapse.

Samples undergo a transition temperature which is different for samples with different ionic strengths. This transition temperature is considered to be the temperature that specific volume exhibits discontinuity. This happens due to the LCST behavior of PNIPAAm which dehydrates and makes the system more hydrophobic after the transition temperature.

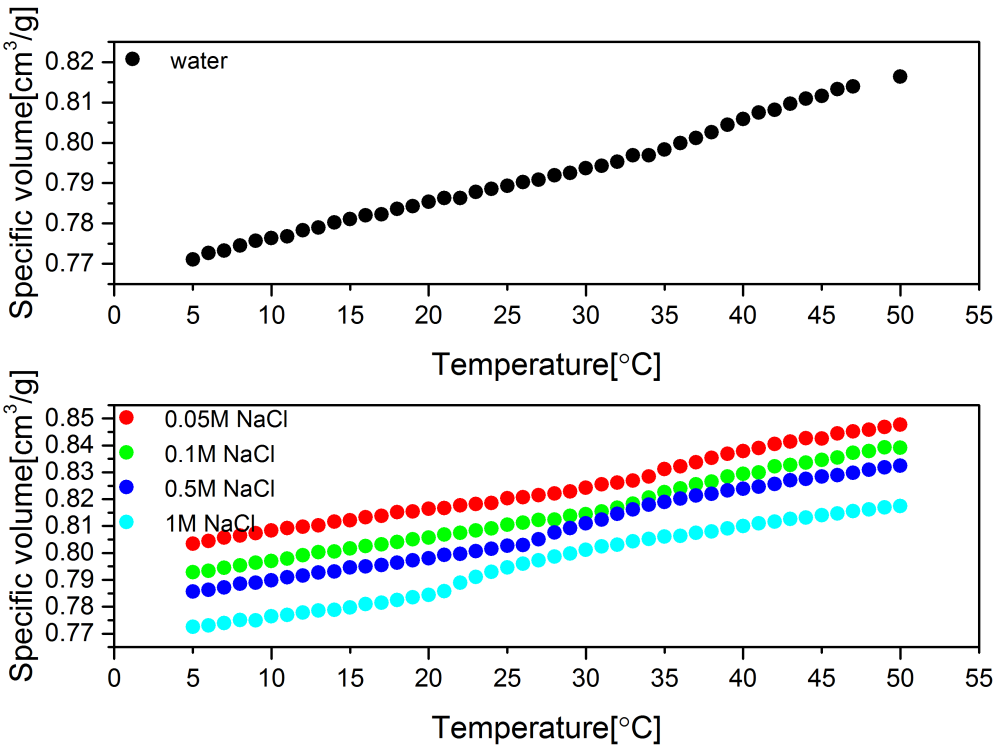

Figure 3.24: Specific volume values of 0.5wt% C_{18}-PEG_{10}-*b*-$PNIPAAm_{54}$-*b*-$PAMPS_{10}$ in water, and saline solutions in a temperature range of 5 to 50 °C

Specific volume of each block provides us with information about the behavior of the polymer. For PNIPAAm homopolymer, density was measured by densitometer and its specific volume was calculated according to Equation 2.6. The specific volumes of C_{18} and PEG have been taken from the work of Sommer and Pedersen. They have claimed that a micellar concentration up to 5% is low enough to avoid the inter-micellar interactions. Therefore the specific volume of PEG is not affected by the concentration and can be used here [58]. As a result, approximate specific volume of PAMPS was calculated. The whole data has been tabulated in Table 3.1.

Table 3.1: Specific volumes of C_{18}, PEG, PNIPAAM, and PAMPS at various temperatures

Temperature [°C]	$V_{C_{18}}$ [cm^3/g]	V_{PEG} [cm^3/g]	$V_{PNIPAAm}$ [cm^3/g]	V_{PAMPS} [cm^3/g]
10	1.243	0.823	0.86664	0.57104
15	1.259	0.8274	0.87038	0.57403
20	1.272	0.8318	0.87445	0.57779
25	1.281	0.8359	0.87842	0.58117
30	1.29	0.8397	0.8821	0.58526
35	1.3	0.8435	0.89626	0.5762
40	1.308	0.8477	0.90195	0.58557
45	1.315	0.852	0.90244	0.59944
50	1.322	0.8561	0.90389	0.6137

Knowing the specific volume of the individual blocks, and extracting the bound coherent scattering length from the NIST Center for Neutron Research website [68], by using Equation 2.9 one can calculate the scattering length density. These values for C_{18}, PEG and PNIPAAm have been taken from the references [12] and it was only calculated for the PAMPS block. These values are further used in SANS fittings and are tabulated in Table 3.2.

Table 3.2: SLD (ρ) of C_{18}, PEG, PNIPAAM, and PAMPS at 25 °C

$\rho_{C_{18}}$ [cm^{-2}]	ρ_{PEG} [cm^{-2}]	$\rho_{PNIPAAm}$[cm^{-2}]	ρ_{PAMPS} [cm^{-2}]
-0.34×10^{10}	0.68×10^{10}	0.85×10^{10}	0.56×10^{10}

3.5 Small Angle Neutron Scattering (SANS)

The q dependencies of the scattering intensity for 0.5wt% C_{18}-PEG_{10}-*b*-$PNIPAAm_{54}$-*b*-$PAMPS_{10}$ solutions with different salt concentrations at different temperatures are studied (double logarithmic plots of intensity vs. q). We intended to probe the possible impact of temperature and ionic strength on the mesoscopic structure. The SANS spectra for different samples exhibit different profiles, which indicate that temperature and ionic strength affect the polymeric association structures. The plotted results are accompanied by their fits when it is possible to have one, once having larger aggregates and when we are near the CP it is not possible to have a proper fit.

Simply by visual inspection, we can see that at low q a strongly-increasing scattering commences above a certain temperature for 0.5wt% solutions of C_{18}-PEG_{10}-*b*-$PNIPAAm_{54}$-*b*-$PAMPS_{10}$. This temperature becomes lower and lower as the salt concentration is increased. We see that for the highest salt concentration (Figure 3.29), the increased scattering has started already at 20 °C, which

is reasonable since the cloud point was measured to 20 °C for this system. Interestingly, in the absence of salt (Figure 3.25), there are some small but highly systematic changes (increased low-q scattering) for each temperature step, but the large change is not seen until above 35 °C, which is the cloud point of the pure polymer in D_2O. For the other samples (Figure 3.26, 3.27, 3.28), there is a clear trend of change between these extremes. Thus the SANS data seem to confirm quite well the turbidity data.

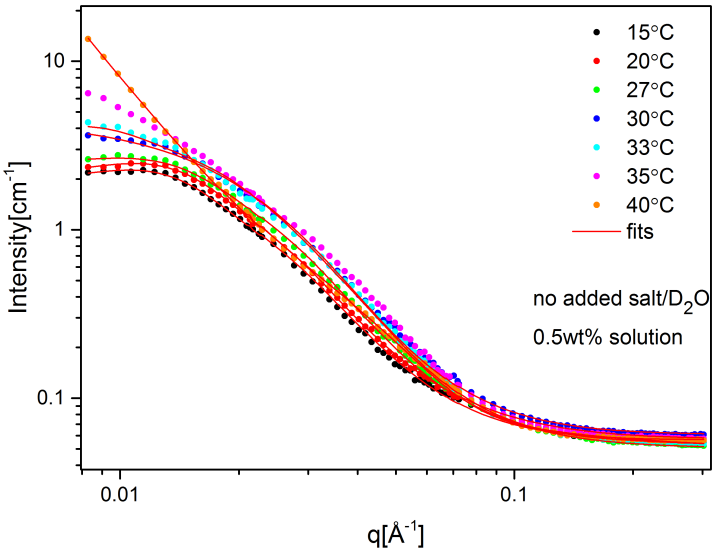

Figure 3.25: SANS scattering profile of 0.5wt% C_{18}-PEG_{10}-*b*-$PNIPAAm_{54}$-*b*-$PAMPS_{10}$ in D_2O at different temperatures fitted by a core-shell model (Equation 2.10)

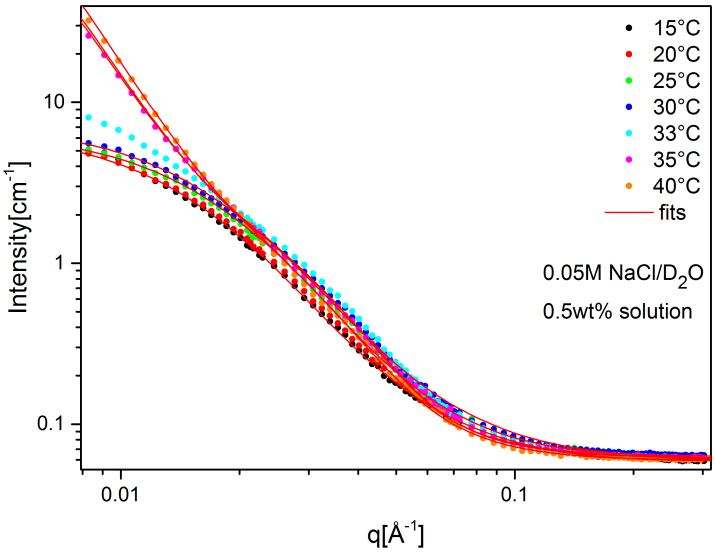

Figure 3.26: SANS scattering profile of 0.5wt% C_{18}-PEG_{10}-*b*-$PNIPAAm_{54}$-*b*-$PAMPS_{10}$ in 0.05M NaCl/D_2O at different temperatures fitted by a core-shell model (Equation 2.10)

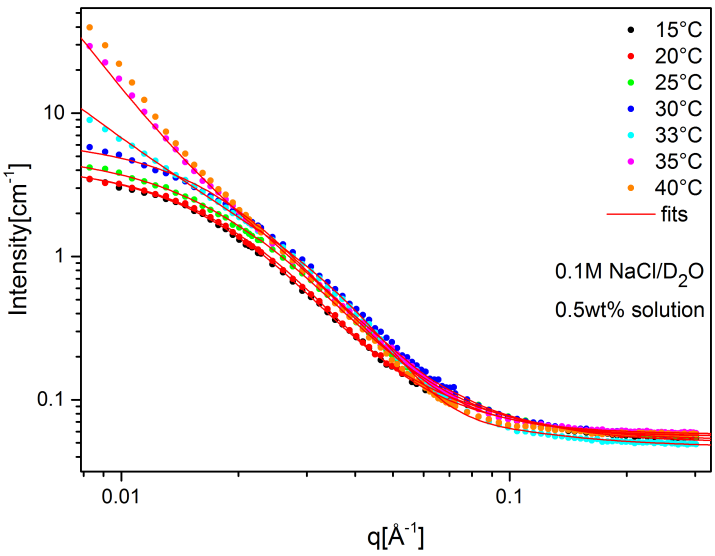

Figure 3.27: SANS scattering profile of 0.5wt% C_{18}-PEG_{10}-*b*-$PNIPAAm_{54}$-*b*-$PAMPS_{10}$ in 0.1M NaCl/D_2O at different temperatures fitted by a core-shell model (Equation 2.10)

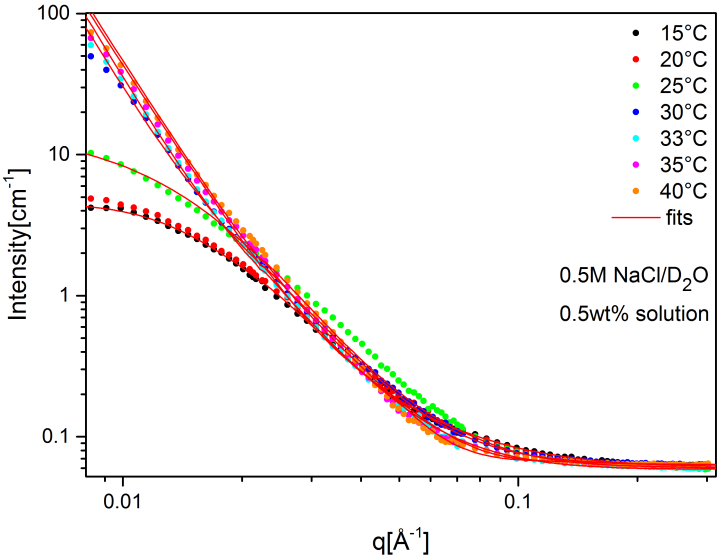

Figure 3.28: SANS scattering profile of 0.5wt% C_{18}-PEG_{10}-*b*-$PNIPAAm_{54}$-*b*-$PAMPS_{10}$ in 0.5M NaCl/D_2O at different temperatures fitted by a core-shell model (Equation 2.10)

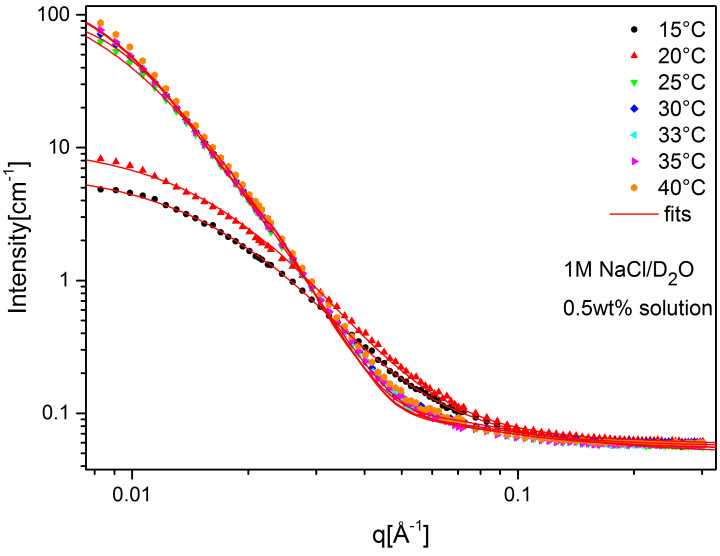

Figure 3.29: SANS scattering profile of 0.5wt% C_{18}-PEG_{10}-*b*-$PNIPAAm_{54}$-*b*-$PAMPS_{10}$ in 1M NaCl/D_2O at different temperatures fitted by a core-shell model (Equation 2.10)

Another way to show the behavior is to select one temperature and see how the different samples with CPs below and above that temperature behave. For the Figure 3.30, we have chosen T=30 °C, being in the middle of all temperatures measured.

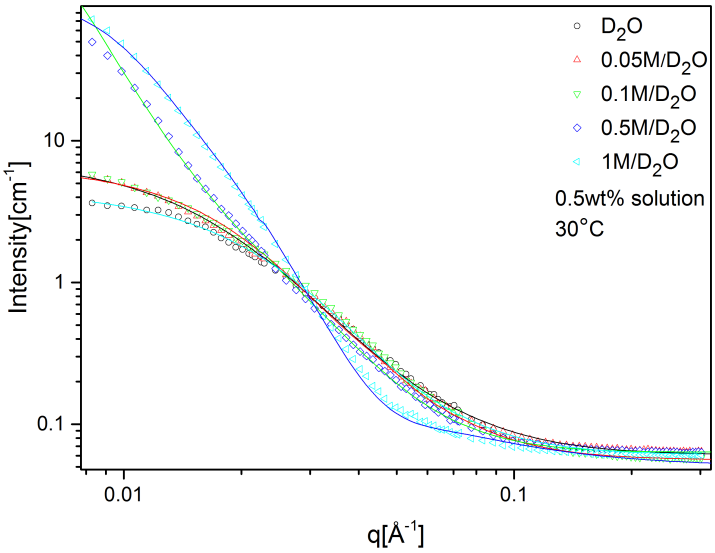

Figure 3.30: SANS scattering profile of 0.5wt% C_{18}-PEG_{10}-*b*-$PNIPAAm_{54}$-*b*-$PAMPS_{10}$ at different ionic strengths in D_2O at 30 °C fitted by a core-shell model (Equation 2.10)

As expected, we now see clearly how samples in 0.5M and 1M D_2O, with CPs below this temperature (27 and 20 °C, respectively), have a 10-fold stronger scattering at low q compared with the others. Samples in pure and 0.05M D_2O have CPs below 30 °C, and show the scattering typical of smaller entities, as mentioned before. The sample in 0.1M D_2O has CP listed at 30 °C, thus we are just at the edge of the transition, but we see that it has not manifested itself yet, and it behaves equal to the sample in 0.05M NaCl.

Another way to plot the data is to select a temperature below the CP for all samples, and see how they behave. In Figure 3.31 we have plotted the samples at T = 15 °C, which is below the lowest CP for these samples (20 °C). We have kept the same y-axis scaling as before, in order to better compare the datasets. In Figure 3.31 the corresponding fits of the plots are also included.

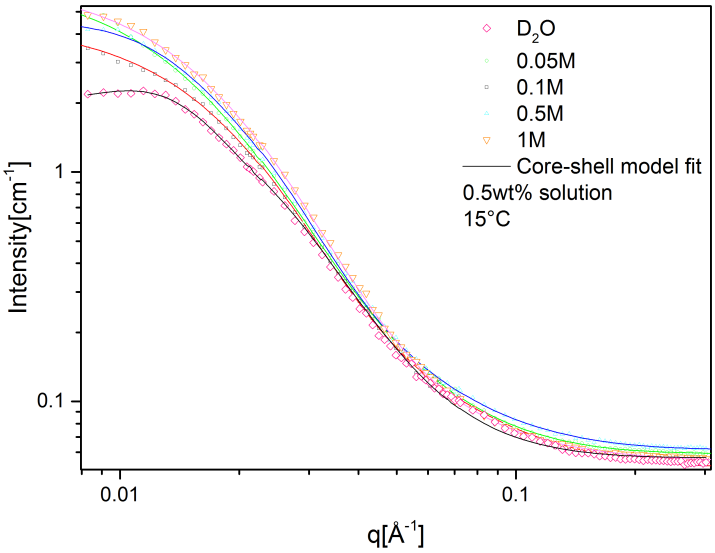

Figure 3.31: SANS scattering profile of 0.5wt% C_{18}-PEG_{10}-*b*-$PNIPAAm_{54}$-*b*-$PAMPS_{10}$ at different ionic strengths in D_2O at 15 °C fitted by a core-shell model (Equation 2.10)

As expected, we see that the scattering patterns are now quite similar for all samples, falling much closer than what was the case in the previous figure. There is near full overlap in the mid- and high-q region. However, sample with no added salt - with the highest CP - shows a slightly different behavior in the lowest q-range, indicating somewhat smaller particles than for the other samples with salt. There are also some minor differences between the samples with salt, and this may be because the conformation can depend slightly on the distance between the actual temperature (15 °C) and the CP for each sample. The fits at 15 °C seem quite good. They are less promising at higher temperatures, that is probably due to formation of large aggregates, clusters and poly-disperse ensembles with variation in size. Thus it is understandable that a good fit is difficult at these higher temperatures. It is probably explainable that just around the CP the fit will never be good, since the system is in a transition, i.e. a somewhat undetermined state.

Finally, we may consider a temperature above the CP for all samples. Below we have plotted the samples at T = 40 °C, which is above the highest CP for these samples (35 °C).

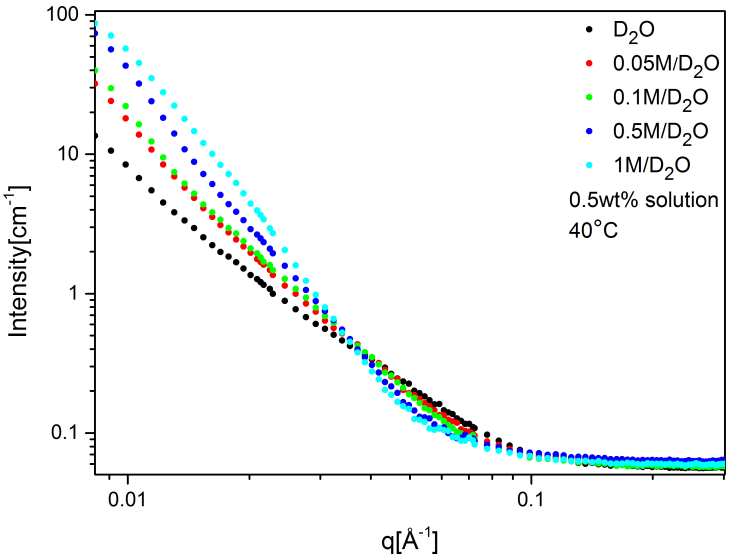

Figure 3.32: SANS scattering profile of 0.5wt% C_{18}-PEG_{10}-*b*-$PNIPAAm_{54}$-*b*-$PAMPS_{10}$ at different ionic strengths in D_2O at 40 °C

Contrary to what was observed at the lowest temperature (1 °C), we now see large differences in the patterns, and that the low-q intensity increases continuously with increasing distance between the actual temperature (40 °C) and the CP for each sample. This is probably because the aggregation tendency is drastically dependent on how far one is above the CP for the sample in question.

The SANS data seem to compare well with the information from turbidity. We see a conversion from micellar-like structures below CP to large aggregates above CP for all samples. Therefore, at a certain temperature, e.g. 30 °C, we see considerable difference in particle size depending on the CP (and thus the ionic strength) of the sample in question. Furthermore, well below the CP for all samples, they show clear similarities with respect to particle size and shape, whereas above the CP they demonstrate large differences, probably due to different degree of stickiness that results in different aggregate sizes.

Structural parameters deduced from the core-shell model for C_{18}-PEG_{10}-*b*-$PNIPAAm_{54}$-*b*-$PAMPS_{10}$ in D_2O at various temperatures are tabulated in Tables 3.3, 3.4, 3.5, 3.6, 3.7. P is the aggregation number, R_m is the overall micellar radius, and R_c is the core radius.

Table 3.3: P (the aggregation number), R_m (the overall micellar radius), and R_c (the core radius) at different temperatures for 0.5wt% C_{18}-PEG_{10}-*b*-$PNIPAAm_{54}$-*b*-$PAMPS_{10}$ in D_2O

Temperature [°C]	P	R_m [Å]	R_c [Å]
15	39	59	14
20	21	62	14
27	21	58	14
30	25	59	15
33	27	22	15
40	17	49	13

Table 3.4: P (the aggregation number), R_m (the overall micellar radius), and R_c (the core radius) at different temperatures for 0.5wt% C_{18}-PEG_{10}-*b*-$PNIPAAm_{54}$-*b*-$PAMPS_{10}$ in 0.05M NaCl- D_2O

Temperature [°C]	P	R_m [Å]	R_c [Å]
15	40	54	17
20	38	52	17
27	39	51	17
30	43	48	17

Table 3.5: P (the aggregation number), R_m (the overall micellar radius), and R_c (the core radius) at different temperatures for 0.5wt% C_{18}-PEG_{10}-*b*-$PNIPAAm_{54}$-*b*-$PAMPS_{10}$ in 0.1M NaCl- D_2O

Temperature [°C]	P	R_m [Å]	R_c [Å]
15	28	47	15
20	26	67	15
27	31	35	17

Table 3.6: P (the aggregation number), R_m (the overall micellar radius), and R_c (the core radius) at different temperatures for 0.5wt% C_{18}-PEG_{10}-*b*-$PNIPAAm_{54}$-*b*-$PAMPS_{10}$ in 0.5M NaCl- D_2O

Temperature [°C]	P	R_m [Å]	R_c [Å]
15	33	90	16
20	38	81	17
27	94	83	23
30	26	44	15
33	25	41	15

Table 3.7: P (the aggregation number), R_m (the overall micellar radius), and R_c (the core radius) at different temperatures for 0.5wt% C_{18}-PEG_{10}-*b*-$PNIPAAm_{54}$-*b*-$PAMPS_{10}$ in 1M NaCl- D_2O

Temperature [$^\circ$C]	P	R_m [Å]	R_c [Å]
15	39.868	59.918	17.317
20	63.026	67.022	20.173

For all samples there seems to be a clear trend in reduction in R_c with increasing temperature, at least from below to above CP (although there is some variation due to noise/statistics) which is reasonable possibly due to the compaction of PNIPAAm with temperature.
The R_m also seems to show a downwards trend (below CP), apart from 0.1M at 20 $^\circ$C, and this is probably reasonable since it follows the behavior of R_c. The aggregation number (P) is a bit more difficult to interpret, but it seems that below CP, it is quite stable (with some noise added), with a rough average value of 30-40 for all samples. Above CP it seems to get very low, but this could just be a problem with the fitting above CP which can be a result of the formation of large micelles and aggregates.

Chapter 4

Conclusion and perspectives

This research was aimed to study the negatively charged thermo-responsive amphiphilic end-capped triblock terpolymer, C_{18}-PEG_{10}-*b*-$PNIPAAm_{54}$-*b*-$PAMPS_{10}$. The polymer was characterized using NMR and AFFFF. The study on the self-assembled polymeric solutions of different ionic-strengths has been conducted by employing zeta potential measurements, turbidimetry, DLS, densitometry and SANS.

Zeta potential measurements depict that at higher temperatures, the charges are pressed out on the surface of micelles and inter-micellar aggregates. Turbidimetry results confirm that the studied polymer, exhibits LCST behavior. At elevated temperatures the hydrogen bonds between the PNIPAAm block of the copolymer and water molecules are weakened or broken up which increases the hydrophobicity of the polymer chains and eventually the aggregates are formed. Since this copolymer is charged, alterations in the ionic strengths of its corresponding solutions will also affect the physical properties of the system through the screening of electrostatic interactions. It has been shown that increasing the ionic strength of copolymer solutions leads to screening out the charges on the polymeric chains and the hydrophobicity of the polymer in solution is enhanced. The higher the salt concentration, the lower is the cloud point. Densitometry measurements disclose that the samples undergo a transition temperature which is different for samples with different ionic strengths. This transition temperature is considered to be the temperature that specific volume deviates from the rising trend and gains much higher value. This happens due to the LCST behavior of PNIPAAm which dehydrates and makes the system more hydrophobic after the transition temperature. Therefore the polymeric associations will collapse and force the water out of the polymeric chain vicinities.

According to the beta values in DLS, at lower temperatures, the system is rather poly-disperse for samples with or without added NaCl. By reaching the LCST, the copolymer complexes start to

contract as the temperature increases. This leads to a decrease of the apparent hydrodynamic radius (R_h). Whereas at elevated temperatures the increased hydrophobicity (due to the breakage of the hydrogen bonds) yields larger aggregates. Moreover, The β values suggest that the intermicellar clusters have a narrow size distribution at high temperatures. Increasing the ionic-strengths, result in compression and collapse of the polymeric chains because of screening of the electrostatic interactions and it has been shown that the hydrodynamic radii (R_h) have been decreased. At higher temperatures, as a result of the breakage of hydrogen bonds, the polymeric chains become stickier and R_h values get higher. Transition temperatures in densitometry and turbiditimetry were almost the same for the polymeric solutions. Both turbidity and DLS results accentuate the competition between contraction and aggregation throughout the temperature range.

The SANS data seem to compare well with the turbidity results. We see a conversion from micelle-like structures below CP to inter-micellar complexes above CP for all samples with different ionic strengths. Therefore, below the CP for all samples, particle sizes and shapes show strong similarities in contrast, above the CP they demonstrate large differences which can be attributed to different degrees of stickiness that result in different aggregate sizes.

The introduced triblock terpolymer in this study has been shown to be a multi-responsive block copolymer, the behavior of which is highly susceptible to alterations in temperature, ionic strength, and concentration. Consequently, this characteristics make the considered triblock copolymer capable of being used in many applications as it was mentioned in chapter 1. Moreover, PEG is recognized for its bio-compatibility and its resistance to protein adsorption and cellular adhesion which helps with its prolonged circulation time [25].

Perspectives

The context of this research was to study a thermo-responsive and ionic-strength responsive amphiphilic block copolymer. To get the complete structural information for complicated polydisperse systems such as the one studied here, combining USANS and SANS data enables us to determine their complex morphologies [69]. To cover a wider q-range it is also interesting to take advantage of static light scattering (SLS) as well.

Other studies can be based on tailoring the amphiphilicity of this class of block copolymers. Studies have been performed on the uncharged diblocks of the same polymer in this study [12], therefore further studies consisting the effect of block length on the structures and behaviors of the solutions seems to be promising. The ionic-strength of the solutions could also be altered using more com-

plex polyelectrolytes. Furthermore, it will be stimulating to study encapsulated hydrophobic drugs or dyes, and characterize their behavior through the applied methods here. Performing the *in vitro* and *in vivo* tests will be interesting as well.

Bibliography

[1] P. Alexandridis, "Amphiphilic copolymers and their applications," *Current Opinion in Colloid & Interface Science*, vol. 1, no. 4, pp. 490–501, 1996.

[2] E. Cabane, X. Zhang, K. Langowska, C. Palivan, and W. Meier, "Stimuli-responsive polymers and their applications in nanomedicine," *Biointerphases*, vol. 7, no. 1-4, pp. 1–27, 2012.

[3] I. W. Wyman and G. Liu, "Micellar structures of linear triblock terpolymers: Three blocks but many possibilities," *Polymer*, vol. 54, no. 8, pp. 1950–1978, 2013.

[4] L. Zhang and A. Eisenberg, "Formation of crew-cut aggregates of various morphologies from amphiphilic block copolymers in solution," *Polymers for Advanced Technologies*, vol. 9, no. 10-11, pp. 677–699, 1998.

[5] J. F. Gohy, "Block copolymer micelles," in *Block Copolymers II* (V. Abetz, ed.), vol. 190 of *Advances in Polymer Science*, book section 48, pp. 65–136, Springer Berlin Heidelberg, 2005.

[6] D. Roy, W. L. A. Brooks, and B. S. Sumerlin, "New directions in thermoresponsive polymers," *Chemical Society Reviews*, vol. 42, no. 17, pp. 7214–7243, 2013.

[7] C. Zhou, M. A. Hillmyer, and T. P. Lodge, "Micellization and micellar aggregation of poly(ethylene-alt-propylene)-b- poly(ethylene oxide)-b-poly(N-isopropylacrylamide) triblock terpolymers in water," *Macromolecules*, vol. 44, no. 6, pp. 1635–1641, 2011.

[8] O. V. Borisov and E. B. Zhulina, "Effect of salt on self-assembly in charged block copolymer micelles," *Macromolecules*, vol. 35, no. 11, pp. 4472–4480, 2002.

[9] S. Liu, J. V. M. Weaver, Y. Tang, N. C. Billingham, S. P. Armes, and K. Tribe, "Synthesis of shell cross-linked micelles with ph-responsive cores using ABC triblock copolymers," *Macromolecules*, vol. 35, no. 16, pp. 6121–6131, 2002.

[10] Y. Bae, S. Fukushima, A. Harada, and K. Kataoka, "Design of environment-sensitive supramolecular assemblies for intracellular drug delivery: Polymeric micelles that are responsive to intracellular pH change," *Angewandte Chemie International Edition*, vol. 42, no. 38, pp. 4640–4643, 2003.

[11] X. L. Yang, Y. L. Luo, F. Xu, and Y. S. Chen, "Thermosensitive mPEG-b-PA-g-PNIPAM comb block copolymer micelles: Effect of hydrophilic chain length and camptothecin release behavior," *Pharmaceutical Research*, vol. 31, no. 2, pp. 291–304, 2014.

[12] Z. Quan, K. Zhu, K. D. Knudsen, B. Nyström, and R. Lund, "Tailoring the amphiphilicity and self-assembly of thermosensitive polymers: end-capped PEG-PNIPAAM block copolymers," *Soft Matter*, vol. 9, no. 45, pp. 10768–10778, 2013.

[13] W. N. Yu, S. X. Liu, H. M. Wang, and R. Tian, "Synthesis and micellization of P(NIPAM-co-HMAM)-b-PEO-b-P(NIPAM-co-HMAM) triblock copolymers," *Journal of Polymer Research*, vol. 19, no. 11, pp. 1–7, 2012.

[14] S. Bayati, K. Zhu, L. T. T. Trinh, A. L. Kjøniksen, and B. Nyström, "Effects of temperature and salt addition on the association behavior of charged amphiphilic diblock copolymers in aqueous solution," *The Journal of Physical Chemistry B*, vol. 116, no. 36, pp. 11386–11395, 2012.

[15] S. Guragain, B. P. Bastakoti, S. i. Yusa, and K. Nakashima, "Stimuli-induced core-corona inversion of micelles of water-soluble poly(sodium 2-(acrylamido)-2-methyl propanesulfonate-b-N-isopropylacrylamide)," *Polymer*, vol. 51, no. 14, pp. 3181–3186, 2010.

[16] C. M. Schilli, M. Zhang, E. Rizzardo, S. H. Thang, Y. K. Chong, K. Edwards, G. Karlsson, and A. H. E. Müller, "A new double-responsive block copolymer synthesized via RAFT polymerization: poly(N-isopropylacrylamide)-block-poly(acrylic acid)," *Macromolecules*, vol. 37, no. 21, pp. 7861–7866, 2004.

[17] Y. Xia, N. A. D. Burke, and H. D. H. Stöver, "End group effect on the thermal response of narrow-disperse poly(N-isopropylacrylamide) prepared by atom transfer radical polymerization," *Macromolecules*, vol. 39, no. 6, pp. 2275–2283, 2006.

[18] H. G. Schild and D. A. Tirrell, "Microcalorimetric detection of lower critical solution temperatures in aqueous polymer solutions," *The Journal of Physical Chemistry*, vol. 94, no. 10, pp. 4352–4356, 1990.

[19] Y. Mi Kyong, S. Yong Kiel, S. C. Chong, and M. L. Young, "Effect of polymer complex formation on the cloud-point of poly(N-isopropyl acrylamide) (PNIPAAm) in the poly(NIPAAm-co-acrylic acid): polyelectrolyte complex between poly(acrylic acid) and poly(allylamine)," *Polymer*, vol. 38, no. 11, pp. 2759–2765, 1997.

[20] G. Masci, M. Diociaiuti, and V. Crescenzi, "ATRP synthesis and association properties of thermoresponsive anionic block copolymers," *Journal of Polymer Science Part A: Polymer Chemistry*, vol. 46, no. 14, pp. 4830–4842, 2008.

[21] R. Pamies, K. Zhu, A. L. Kjøniksen, and B. Nyström, "Thermal response of low molecular weight poly-(N-isopropylacrylamide) polymers in aqueous solution," *Polymer Bulletin*, vol. 62, no. 4, pp. 487–502, 2009.

[22] M. A. Behrens, M. Lopez, A. L. Kjøniksen, K. Zhu, B. Nyström, and J. S. Pedersen, "Structure and interactions of charged triblock copolymers studied by small-angle X-ray scattering: dependence on temperature and charge screening," *Langmuir*, vol. 28, no. 2, pp. 1105–1114, 2012.

[23] S. Zhou and B. Chu, "Synthesis and volume phase transition of poly(methacrylic acid-co-N-isopropylacrylamide) microgel particles in water," *The Journal of Physical Chemistry B*, vol. 102, no. 8, pp. 1364–1371, 1998.

[24] A. L. Kjøniksen, M. T. Calejo, K. Zhu, A. M. S. Cardoso, M. C. P. De Lima, A. S. Jurado, B. Nyström, and S. A. Sande, "Sustained release of naltrexone from poly(N-isopropylacrylamide) microgels," *Journal of Pharmaceutical Sciences*, vol. 103, no. 1, pp. 227–234, 2014.

[25] S. Qin, Y. Geng, D. E. Discher, and S. Yang, "Temperature-controlled assembly and release from polymer vesicles of poly(ethylene oxide)-block- poly(N-isopropylacrylamide)," *Advanced Materials*, vol. 18, no. 21, pp. 2905–2909, 2006.

[26] M. T. Calejo, S. A. Sande, and B. Nyström, "Thermoresponsive polymers as gene and drug delivery vectors: Architecture and mechanism of action," *Expert Opinion on Drug Delivery*, vol. 10, no. 12, pp. 1669–1686, 2013.

[27] B. Brugger and W. Richtering, "Magnetic, thermosensitive microgels as stimuli-responsive emulsifiers allowing for remote control of separability and stability of oil in water-emulsions," *Advanced Materials*, vol. 19, no. 19, pp. 2973–2978, 2007.

[28] I. Teraoka, *Polymer Solutions: An Introduction to Physical Properties*. Wiley, 2001.

[29] Y. Bae, H. Cabral, and K. Kataoka, "Block copolymer micelles for drug delivery in nanoscience," in *Block Copolymers in Nanoscience* (M. Lazzari, G. Liu, and S. Lecommandoux, eds.), book section 4, pp. 73–89, Wiley-VCH Verlag GmbH & Co. KGaA, 2008.

[30] C. A. Fustin, V. Abetz, and J. F. Gohy, "Triblock terpolymer micelles: A personal outlook," *The European Physical Journal E*, vol. 16, no. 3, pp. 291–302, 2005.

[31] R. Lund, L. Willner, and D. Richter, "Kinetics of block copolymer micelles studied by small-angle scattering methods," in *Controlled Polymerization and Polymeric Structures* (A. Abe, K. S. Lee, L. Leibler, and S. Kobayashi, eds.), vol. 259 of *Advances in Polymer Science*, book section 204, pp. 51–158, Springer International Publishing, 2013.

[32] S. Förster and T. Plantenberg, "From self-organizing polymers to nanohybrid and biomaterials," *Angewandte Chemie International Edition in English*, vol. 41, no. 5, pp. 689–714, 2002.

[33] K. Kataoka, A. Harada, and Y. Nagasaki, "Block copolymer micelles for drug delivery: Design, characterization and biological significance," *Advanced Drug Delivery Reviews*, vol. 47, no. 1, pp. 113–131, 2001.

[34] M. A. Behrens, A. L. Kjøniksen, K. Zhu, B. Nyström, and J. S. Pedersen, "Small-angle X-ray scattering study of charged triblock copolymers as a function of polymer concentration, temperature, and charge screening," *Macromolecules*, vol. 45, no. 1, pp. 246–255, 2012.

[35] I. Astafieva, X. F. Zhong, and A. Eisenberg, "Critical micellization phenomena in block polyelectrolyte solutions," *Macromolecules*, vol. 26, no. 26, pp. 7339–7352, 1993.

[36] K. Yu, L. Zhang, and A. Eisenberg, "Novel morphologies of crew-cut aggregates of amphiphilic diblock copolymers in dilute solution," *Langmuir*, vol. 12, no. 25, pp. 5980–5984, 1996.

[37] A. J. de Graaf, K. W. M. Boere, J. Kemmink, R. G. Fokkink, C. F. van Nostrum, D. T. S. Rijkers, J. van der Gucht, H. Wienk, M. Baldus, E. Mastrobattista, T. Vermonden, and W. E. Hennink, "Looped structure of flowerlike micelles revealed by 1H NMR relaxometry and light scattering," *Langmuir*, vol. 27, no. 16, pp. 9843–9848, 2011.

[38] G. Riess, "Micellization of block copolymers," *Progress in Polymer Science*, vol. 28, no. 7, pp. 1107–1170, 2003.

[39] M. W. Matsen and F. S. Bates, "Origins of complex self-assembly in block copolymers," *Macromolecules*, vol. 29, no. 23, pp. 7641–7644, 1996.

[40] Y. Wang, H. Xu, and X. Zhang, "Tuning the amphiphilicity of building blocks: Controlled self-assembly and disassembly for functional supramolecular materials," *Advanced Materials*, vol. 21, no. 28, pp. 2849–2864, 2009.

[41] K. Thuresson, S. Nilsson, A. L. Kjøniksen, H. Walderhaug, B. Lindman, and B. Nyström, "Dynamics and rheology in aqueous solutions of associating diblock and triblock copolymers of the same type," *The Journal of Physical Chemistry B*, vol. 103, no. 9, pp. 1425–1436, 1999.

[42] A. Rösler, G. W. M. Vandermeulen, and H. A. Klok, "Advanced drug delivery devices via self-assembly of amphiphilic block copolymers," *Advanced Drug Delivery Reviews*, vol. 53, no. 1, pp. 95–108, 2012.

[43] J. F. Gohy, "Stimuli-responsive block copolymer assemblies," in *Block Copolymers in Nanoscience* (M. Lazzari, G. Liu, and S. Lecommandoux, eds.), book section 5, pp. 91–116, Wiley-VCH Verlag GmbH & Co. KGaA, 2008.

[44] A. L. Kjøniksen, K. Zhu, M. A. Behrens, J. S. Pedersen, and B. Nyström, "Effects of temperature and salt concentration on the structural and dynamical features in aqueous solutions of charged triblock copolymers," *Journal of Physical Chemistry B*, vol. 115, no. 10, pp. 2125–2139, 2011.

[45] S. Mishra, A. De, and S. Mozumdar, "Synthesis of thermoresponsive polymers for drug delivery," in *Drug Delivery System* (K. K. Jain, ed.), vol. 1141 of *Methods in Molecular Biology*, book section 4, pp. 77–101, Springer New York, 2014.

[46] J. Heyda, S. Soll, J. Yuan, and J. Dzubiella, "Thermodynamic description of the LCST of charged thermoresponsive copolymers," *Macromolecules*, vol. 47, no. 6, pp. 2096–2102, 2014.

[47] E. S. Gil and S. M. Hudson, "Stimuli-reponsive polymers and their bioconjugates," *Progress in Polymer Science*, vol. 29, no. 12, pp. 1173–1222, 2004.

[48] H. Dautzenberg, Y. Gao, and M. Hahn, "Formation, structure, and temperature behavior of polyelectrolyte complexes between ionically modified thermosensitive polymers," *Langmuir*, vol. 16, no. 23, pp. 9070–9081, 2000.

[49] X. Wang, X. Qiu, and C. Wu, "Comparison of the coil-to-globule and the globule-to-coil transitions of a single poly(N-isopropylacrylamide) homopolymer chain in water," *Macromolecules*, vol. 31, no. 9, pp. 2972–2976, 1998.

[50] C. Wu and X. Wang, "Globule-to-coil transition of a single homopolymer chain in solution," *Physical Review Letters*, vol. 80, no. 18, pp. 4092–4094, 1998.

[51] R. Motokawa, S. Koizumi, M. Annaka, T. Nakahira, and T. Hashimoto, "Ultra-small- and small-angle neutron scattering studies of self-assembly in poly(N-isopropylacrylamide)-block-poly (ethylene glycol) aqueous solution," in *Scattering Methods and the Properties of Polymer Materials* (N. Stribeck and B. Smarsly, eds.), vol. 130 of *Progress in Colloid and Polymer Science*, book section 11, pp. 85–96, Springer Berlin Heidelberg, 2005.

[52] X. Shi, J. Li, C. Sun, and S. Wu, "The aggregation and phase separation behavior of a hydrophobically modified poly(N-isopropylacrylamide)," *Colloids and Surfaces A: Physicochemical and Engineering Aspects*, vol. 175, no. 1-2, pp. 41–49, 2000.

[53] Y. Zhang, W. Lin, R. Jing, and J. Huang, "Effect of block sequence on the self-assembly of ABC terpolymers in selective solvent," *The Journal of Physical Chemistry B*, vol. 112, no. 51, pp. 16455–16460, 2008.

[54] J. D. Clogston and A. K. Patri, "Zeta potential measurement," in *Characterization of Nanoparticles Intended for Drug Delivery* (S. E. McNeil, ed.), vol. 697 of *Methods in Molecular Biology*, book section 6, pp. 63–70, Humana Press, 2011.

[55] H. Jonassen, A. L. Kjøniksen, and M. Hiorth, "Effects of ionic strength on the size and compactness of chitosan nanoparticles," *Colloid and Polymer Science*, vol. 290, no. 10, pp. 919–929, 2012.

[56] A. L. Kjøniksen, A. Laukkanen, C. Galant, K. D. Knudsen, H. Tenhu, and B. Nyström, "Association in aqueous solutions of a thermoresponsive PVCL-g-C11EO42 copolymer," *Macromolecules*, vol. 38, no. 3, pp. 948–960, 2005.

[57] B. Nyström, K. Thuresson, and B. Lindman, "Rheological and dynamic light-scattering studies on aqueous solutions of a hydrophobically modified nonionic cellulose ether and its unmodified analog," *Langmuir*, vol. 11, no. 6, pp. 1994–2002, 1995.

[58] C. Sommer, J. S. Pedersen, and P. C. Stein, "Apparent specific volume measurements of poly(ethylene oxide), poly(butylene oxide), poly(propylene oxide), and octadecyl chains in the micellar state as a function of temperature," *The Journal of Physical Chemistry B*, vol. 108, no. 20, pp. 6242–6249, 2004.

[59] E. Halit, "Density measurement," in *The Measurement, Instrumentation and Sensors Handbook on CD-ROM*, book section 21, CRC Press, 1999.

[60] "Small-angle neutron scattering," in *Modern Techniques for Characterizing Magnetic Materials* (Y. Zhu, ed.), book section 2, pp. 65–105, Springer US, 2005.

[61] R. A. Ramli, W. A. Laftah, and S. Hashim, "Core-shell polymers: a review," *RSC Advances*, vol. 3, no. 36, pp. 15543–15565, 2013.

[62] A. Guinier and G. Fournet, *Small-angle scattering of X-rays*. Structure of matter series, Wiley, 1955.

[63] "Scattering length density calculator @http://www.ncnr.nist.gov/resources/sldcalc.html," Jan. 2014.

[64] J. S. Pedersen, C. Svaneborg, K. Almdal, I. W. Hamley, and R. N. Young, "A small-angle neutron and X-ray contrast variation scattering study of the structure of block copolymer micelles: corona shape and excluded volume interactions," *Macromolecules*, vol. 36, no. 2, pp. 416–433, 2003.

[65] Y. L. Luo, L. L. Zhang, and F. Xu, "Synthesis, micellization and caffeine drug release kinetics of novel PBMA-b-PNIPAAm block polymer brushes," *Chemical Engineering Journal*, vol. 189-190, pp. 431–442, 2012.

[66] E. Karjalainen, N. Chenna, P. Laurinmaki, S. J. Butcher, and H. Tenhu, "Diblock copolymers consisting of a polymerized ionic liquid and poly(N-isopropylacrylamide). effects of pnipam block length and counter ion on self-assembling and thermal properties," *Polymer Chemistry*, vol. 4, pp. 1014–1024, 2013.

[67] N. Beheshti, K. Zhu, A. L. Kjøniksen, K. D. Knudsen, and B. Nyström, "Characterization of temperature-induced association in aqueous solutions of charged ABCBA-type pentablock tercopolymers," *Soft Matter*, vol. 7, pp. 1168–1175, 2011.

[68] "Neutron scattering lengths and cross sections @http://www.ncnr.nist.gov/resources/n-lengths/list.html," Nov. 1999.

[69] R. Triolo and M. Agamalian, "The combined ultra-small- and small-angle neutron scattering (USANS/SANS) technique for earth sciences," in *Neutron Applications in Earth, Energy and Environmental Sciences* (L. Liang, R. Rinaldi, and H. Schober, eds.), Neutron Scattering Applications and Techniques, book section 20, pp. 571–594, Springer US, 2009.